AFWL-TR-87-102

AFWL-TR-
87-102

MAGNETICALLY SUPPRESSED 1.315 μm ATOMIC IODINE ABSORPTION

Capt Mark E. Daily, et al

September 1988

Final Report

AIR FORCE WEAPONS LABORATORY
Air Force Systems Command
Kirtland Air Force Base, NM 87117-6008

UNCLASSIFIED
SECURITY CLASSIFICATION OF THIS PAGE

ADA201 254

REPORT DOCUMENTATION PAGE

Form Approved OMB No. 0704-0188

1a. REPORT SECURITY CLASSIFICATION UNCLASSIFIED	1b. RESTRICTIVE MARKINGS
2a. SECURITY CLASSIFICATION AUTHORITY	3. DISTRIBUTION/AVAILABILITY OF REPORT Approved for public release; distribution unlimited.
2b. DECLASSIFICATION/DOWNGRADING SCHEDULE	
4. PERFORMING ORGANIZATION REPORT NUMBER(S) AFWL-TR-87-102	5. MONITORING ORGANIZATION REPORT NUMBER(S)
6a. NAME OF PERFORMING ORGANIZATION Air Force Weapons Laboratory 6b. OFFICE SYMBOL (If applicable) ARBI	7a. NAME OF MONITORING ORGANIZATION
6c. ADDRESS (City, State, and ZIP Code) Kirtland Air Force Base, NM 87117-6008	7b. ADDRESS (City, State, and ZIP Code)
8a. NAME OF FUNDING/SPONSORING ORGANIZATION 8b. OFFICE SYMBOL (If applicable)	9. PROCUREMENT INSTRUMENT IDENTIFICATION NUMBER
8c. ADDRESS (City, State, and ZIP Code)	10. SOURCE OF FUNDING NUMBERS PROGRAM ELEMENT NO. 62601F; PROJECT NO. 3326; TASK NO 1U; WORK UNIT ACCESSION NO. 01

11. TITLE (Include Security Classification)
MAGNETICALLY SUPPRESSED 1.315 μm ATOMIC IODINE ABSORPTION

12. PERSONAL AUTHOR(S)
Daily, M.E., Capt, USAF; Highland, R.G.; Johnson, D.E., Capt, USAF; Hager, G.D.; Hanko, L.;

13a. TYPE OF REPORT	13b. TIME COVERED	14. DATE OF REPORT (Year, Month, Day)	15. PAGE COUNT
Final	FROM 1Jan86 TO 31May87	1988 September	76

16. SUPPLEMENTARY NOTATION

17. COSATI CODES			18. SUBJECT TERMS (Continue on reverse if necessary and identify by block number)
FIELD	GROUP	SUB-GROUP	
20	03		Magnetic field, Zeeman splitting, Absorption, Hyperfine levels, Atomic iodine, Pressure broadening. (oxygen)
20	05		

19. ABSTRACT (Continue on reverse if necessary and identify by block number)

The influence of a magnetic field on absorption of 1.315 μm radiation by iodine atoms has been investigated using the output from a C_3F_7I photodissociation laser. Atomic iodine was created by thermal dissociation of molecular iodine in a sealed fused silica absorption cell. The cell was placed inside a solenoidal coil creating a longitudinal magnetic field. Absorption of 1.315 μm radiation by iodine atoms was reduced by the Zeeman splitting of the hyperfine levels. The amount of absorption reduction was essentially the same for total cell pressures below 22.9 torr over the range of temperatures studied (823 K to 873 K). At a total cell pressure of 66.7 torr, however, pressure broadening of the magnetic hyperfine transition line-widths decreased the effect of the magnetic field on the absorption.

20. DISTRIBUTION/AVAILABILITY OF ABSTRACT ☒ UNCLASSIFIED/UNLIMITED ☐ SAME AS RPT. ☐ DTIC USERS	21. ABSTRACT SECURITY CLASSIFICATION UNCLASSIFIED
22a. NAME OF RESPONSIBLE INDIVIDUAL Daniel E. Johnson, Capt, USAF	22b. TELEPHONE (Include Area Code) (505) 846-4504 22c. OFFICE SYMBOL ARBI

DD Form 1473, JUN 86 Previous editions are obsolete.

SECURITY CLASSIFICATION OF THIS PAGE
UNCLASSIFIED

12. PERSONAL AUTHORS (Continued)

O'Loughlin, J.P.; and Dunkle, E.

CONTENTS

FIGURES

TABLES

1. INTRODUCTION

Atomic iodine lasers produce infrared radiation at a wavelength of 1.315 μm. The absorption of this radiation by iodine atoms can be influenced by the presence of a magnetic field which splits the atomic energy levels. The splitting of energy levels in an atom or molecule, because of a magnetic field, is known as the Zeeman effect. The purpose of this work was to investigate the influence of a magnetic field on the absorption of 1.315 μm radiation by iodine atoms.

A continuous wave (CW) C_3F_7I photodissociation laser, operating on the 1.315 μm laser transition of atomic iodine, was directed through an absorption cell containing ground state atomic iodine. The atomic iodine was created in the ground state by thermally dissociating molecular iodine in the absorption cell. A portion of the laser beam was split off before it entered the absorption cell. The ratio of the intensities of the transmitted beam and the reference beam was used to determine the absorption in the cell for various temperatures, pressures, and magnetic field strengths.

Both molecular and atomic iodine have been extensively studied for the past century. Since 1964, when lasing was demonstrated on the $^2P_{1/2} \rightarrow {}^2P_{3/2}$ transition of atomic iodine (Ref. 1), the laser transition has been the subject of many studies. One of the main inspirations for this work was the study titled: "Atomic Absorption of Thermally Dissociated Iodine for Laser Applications"(Ref. 2) in which an iodine laser was used to probe a heated absorption cell containing atomic iodine produced by thermal dissociation of molecular iodine. In that work a pulsed iodine laser was used, but magnetic effects were not investigated. Another study (Ref. 3) calculated the Zeeman splitting structure of the energy levels in the atomic iodine laser transition and provided a model for identifying the spectral components of the $^2P_{1/2} \rightarrow {}^2P_{3/2}$ transition in a magnetic field.

In the next section, theoretical aspects of the thermal dissociation of molecular iodine, the energy level structure of atomic iodine, the Zeeman effect, and absorption with and without a magnetic field are discussed. The third section is devoted to a detailed description of the experimental apparatus including the laser, absorption cell, magnetic coil, and data

collection apparatus. Computer programs (presented in Appendices A and B), for calculating the magnetic field arising from the solenoidal coil and for data acquisition and reduction are also discussed in the third section. Experimental results are reported and discussed in the fourth section. Conclusions from these data and some recommendations for improving the experimental procedure are presented in the last section.

2.0 THEORY

2.1 THERMAL DISSOCIATION OF MOLECULAR IODINE

At room temperature (300 K) and standard atmospheric pressure (760 torr*) iodine is a solid with an equilibrium vapor pressure of 0.372 torr. The vapor pressure of many substances may be calculated using the equation

$$\log_{10}P = AT^{-1} + B\log T + CT + D \qquad (1)$$

where P is the equilibrium vapor pressure in torr, and T is the temperature in Kelvin. Here A, B, C, and D are constants which depend on the particular substance and the temperature range of the calculations. For iodine, A = -3578, B = -2.51, C = 0, and D = 17.715 torr, for temperatures between 298 K and 386 K (Ref. 4). Table 1 gives calculated vapor pressures for various temperatures of interest within this range.

The following discussion on the thermal dissociation of molecular iodine is concerned with calculating the number density of atomic iodine at a given temperature and vapor pressure of I_2. This discussion is outlined in Ref. 2, but greater detail is presented here. Many of the equations and specific data for iodine are taken from Ref. 5. The bulk of the discussion is taken from Ref. 6.

Ground state molecular iodine, I_2 ($X^1\Sigma^+$), has a dissociation energy of 1.54 eV. The dissociation products are two ground state iodine atoms denoted as $I(^2P_{3/2})$ (Ref. 5). The thermal dissociation of molecular iodine into ground state atomic iodine can be represented by the reaction,

$$I_2 \rightleftharpoons I + I \qquad (2)$$

At temperatures near 300 K, most of the molecules are in the lowest vibrational state. The extent of molecular dissociation at this temperature is negligible. Given the vapor pressure at a given temperature, the number density of iodine molecules can be calculated using the ideal gas law:

*1 torr = 1.33×10^2 Pascal

TABLE 1. Calculated I_2 vapor pressure using Eq. 1.

Temperature K	Temperature °C	Vapor Pressure (torr)
298	25	0.315
300	27	0.372
310	37	0.831
320	47	1.76
330	57	3.56
340	67	6.88
350	77	12.8
360	87	22.9
370	97	39.7
380	107	66.7

$$\frac{n(I_2)}{V} = \frac{P(I_2)}{kT} \tag{3}$$

where $n(I_2)$ is the number of iodine molecules, V is the volume in cm^3, T is the temperature in Kelvin, $P(I_2)$ is the vapor pressure of I_2 in torr, and k is Boltzmann's constant (1.0359×10^{-19} torr cm^3/K or $1.3807 \times 10^{-23} J/K$).

In general, the total pressure (P_T) consists of the partial pressure of iodine atoms, P(I), and the partial pressure of iodine molecules, $P(I_2)$, where $P_T = P(I) + P(I_2)$. The equilibrium constant K_p is defined as

$$K_p = \frac{P(I)\ P(I)}{P(I_2)} = \frac{[P(I)]^2}{P(I_2)} \tag{4}$$

where K_p depends only on temperature. Values of K_p can be calculated from theoretical considerations or obtained experimentally. To calculate K_p, note that from Eq. 3:

$$P(I_2) = kT \frac{n(I_2)}{V} \tag{5}$$

Similarly,

$$P(I) = kT \frac{n(I)}{V} \tag{6}$$

Substituting these expressions into Eq. 4 gives

$$K_p = \frac{kT[n(I)]^2}{V\ n(I_2)} \tag{7}$$

By the law of mass action, Eq. 7 becomes

$$K_p = \frac{kT[Q(I)]^2}{VQ(I_2)}\ e^{-E/kT} \tag{8}$$

where Q(I) is the partition function of an iodine atom and $Q(I_2)$ is the partition function of an iodine molecule. Here E is the energy difference between the ground state atom and the lowest quantum state of the diatomic molecule (also known as the dissociation energy) which is 1.54 eV for iodine (Ref. 5). The partition function for a free iodine atom is

$$Q(I) = \frac{V(2\pi\ M_I kT)^{3/2}}{h^3}\ e_{g_I}\ n_{g_I} \tag{9}$$

where M_I is the atomic mass (127 amu = 2.11 x 10^{-25} kg), h is Planck's constant (6.626 x 10^{-34}J s), e_{g_I} is the electron spin weight factor (2J + 1 = 4) and n_{g_I} is the nuclear spin weight factor (2I + 1 = 6) (Ref. 6).

The partition function for the molecule consists of translational, vibrational, rotational and electronic factors. At low temperatures, these factors are all separable and, to a good approximation, the vibrational part can be modeled by a harmonic oscillator. At higher temperatures, the molecular vibrations are no longer harmonic but rather anharmonic. The rotation of the molecule produces an additional stretching force along the internuclear axis that is dependent upon the velocity of rotation. In addition, the change in the internuclear separation has a significant effect on the moment of inertia of the molecule in higher vibrational states. If these high temperature effects are included, a reasonably accurate approximation of the molecular partition function can be obtained. To do this, a functional form of the potential energy curve must be chosen. The Morse potential function has been used in the development of a high temperature partition function (Ref. 6). The Morse potential function from Ref. 5 is given by

$$U(r) = D_e[1-e^{-a(r-r_e)}]^2 \tag{10}$$

where D_e is the dissociation energy and is equal to

$$D_e = \frac{\omega_e^2}{4\omega_e x_e} = 3.693 \times 10^{-19}\text{J} \tag{11}$$

The equilibrium nuclear separation is denoted by r_e and the constant a is given by

$$a = \left(\frac{8\pi^2 c\mu\omega_e x_e}{h}\right)^{\frac{1}{2}} = 1.5270 \times 10^{10}\text{m}^{-1} \tag{12}$$

The spectroscopic constants ω_e and $\omega_e x_e$ are 214.54 cm^{-1} and 0.61897cm^{-1}, respectively (Ref. 7). The reduced mass, μ, of the iodine molecule is $M_{I/2}$ or 1.0545 x 10^{-25}kg.

Using the Morse potential function, the partition function can be written as

$$Q(I_2) = \frac{V(4\pi M_I kT)^{3/2}}{h^3} \times Q_{VR} \times \frac{{}^e g_{I_2} ({}^n g_I)^2}{s} \tag{13}$$

where Q_{VR} is the vibration-rotation partition function,

$$Q_{VR}(T) = \frac{1}{\eta(1-e^{-u})} \left[1 + \frac{\eta}{3} + \frac{8\gamma^2}{\eta} + \frac{\delta}{e^{u-1}} + \frac{2\chi u}{(e^{u-1})^2}\right] \tag{14}$$

The quantities in Eq. 14 are defined as follows:

$$\eta = \frac{B_e hc}{kT}(1-\delta/2) = \frac{5.3653 \times 10^{-2}}{T} \tag{15}$$

$$\delta = \frac{\alpha_e}{B_e} = \frac{6B_e}{\tilde{\nu}_e}\left[\left(\frac{\nu_e \chi}{B_e}\right)^{\frac{1}{2}} - 1\right] = 3.2077 \times 10^{-3} \tag{16}$$

$$B_e = \frac{\eta}{8\pi^2 Ac} = 3.735 m^{-1} \tag{17}$$

$$\tilde{\nu}_e = \frac{a}{2\pi c}\left(\frac{2D_e}{\mu}\right)^{\frac{1}{2}} = 2.1454 \times 10^4 m^{-1} \tag{18}$$

$$\chi = \frac{h\tilde{\nu}_e c}{4D_e} = 2.885 \times 10^{-3} \tag{19}$$

$$\gamma = \frac{B_e}{\tilde{\nu}_e} = 1.7409 \times 10^{-4} \tag{20}$$

$$u = \frac{h\nu}{kT}(1 - 2\chi) = \frac{306.906}{T} \tag{21}$$

where

$$\nu = \tilde{\nu}_e c = 6.432 \times 10^{12} Hz$$

$$\alpha_e = \frac{6(\omega_e x_e B_e^3)^{\frac{1}{2}}}{\omega_e} - \frac{6B_e^2}{\omega_e} = 1.198 \times 10^{-2} m^{-1} \tag{22}$$

$$A = \mu r_e^2 = (1.0545 \times 10^{-25} kg)(2.666 \times 10^{-10} m)^2 \tag{23}$$

The terms α_e and B_e are rotational constants; υ is another expression for ω_e and χ is the anharmonicity constant.

Equations 13 through 21 and Eq. 23 are taken from Ref. 6 and Eq. 22 from Ref. 5. The symmetry number s in Eq. 13 has a value of 2 for the iodine molecule.

If Eq. 13 (the molecular partition function) and Eq. 9 (the atomic partition function) are substituted into Eq. 8, the nuclear spin weight factors and volume factors cancel. The expression for K_p then becomes

$$K_p = \frac{(2\pi\mu)^{3/2}(kT)^{5/2}}{h^3} \left(\frac{(e g_I)^2 s}{(e g_I)\, Q_{VR}}\right) e^{-E/kT} \tag{24}$$

The electron spin weight factor for molecular iodine, $e g_{I_2}$, is equal to one. Using this expression, values of K_p were calculated for iodine at temperatures from 732 K to 1173 K (Ref. 2). These values, as well as experimentally determined values given in Refs. 8 and 9, are listed in Table 2. The agreement between the calculated and measured values attests to the validity of the approximations used in calculating K_p even at temperatures up to 1000 K.

The number density of iodine atoms can be found using K_p, the temperature, and the total pressure. Letting $N(I) = n(I)/V$ and $N(I_2) = n(I_2)/V$ (the number densities of iodine atoms and molecules respectively), the total number of particles per cubic centimeter is then

$$N_T = N(I) + N(I_2) \tag{25}$$

From the ideal gas law and Eq. 7, Eq. 25 becomes

$$\frac{kT}{K_p}\,[N(I)]^2 + N(I) - \frac{P_T}{kT} = 0 \tag{26}$$

Solving this quadratic equation for N(I) gives

$$N(I) = \frac{K_p}{2kT}\left[(1 + 4P_T/K_p)^{\frac{1}{2}} - 1\right] \tag{27}$$

TABLE 2. Calculated and experimental values of K_p.

Temperature (K)	K_p (torr)			
	Calculated		Experimental	
	Reference 2	This Work	Reference 8	Reference 9
473	-	*4.10×10^{-7}	-	-
732	*4.00×10^{-3}	-	3.93×10^{-3}	-
794	*1.86×10^{-2}	-	1.80×10^{-2}	-
823	*4.50×10^{-2}	4.408×10^{-2}	4.16×10^{-2}	-
848	*7.90×10^{-2}	-	7.31×10^{-2}	-
873	*1.62×10^{-1}	1.590×10^{-1}	1.33×10^{-1}	1.38×10^{-1}
898	*2.20×10^{-1}	-	2.20×10^{-1}	-
973	*1.43	1.3984	-	1.37
1023	*3.61	-	-	-

NOTE: Starred values were used to calculate N(I) in Table 3.

Results of calculations using this equation are shown in Table 3. The starred values of K_p in Table 2 were used in these calculations.

For a diatomic molecule to strongly emit or absorb infrared radiation through a change in its vibrational and/or rotational state, the dipole moment of the molecule must be nonzero. Iodine, being a homonuclear diatomic molecule, has no dipole moment and does not emit or absorb vibrational-rotational infrared radiation (Ref. 5). In an absorption cell containing only atomic and molecular iodine, only atomic iodine will absorb or emit 1.315 μm radiation. Before calculating the theoretical absorption of atomic iodine under various conditions, it is useful to review its atomic structure.

2.2 ENERGY LEVEL STRUCTURE OF ATOMIC IODINE

Iodine has an atomic number of 53 and the naturally occurring isotope has an atomic weight of 127. Like the other halogens (fluorine, chlorine, bromine and astatine), it has an incomplete outer electron subshell. The electron configuration of the ground state of iodine can be written as $[Kr]5s^24d^{10}5p^5$. The 36 inner electrons are configured similarly to the krypton atom. The outer 17 electrons completely fill the 5s and 4d subshells leaving the 5p subshell with five of the six electrons needed to fill it. The orbital angular momentum quantum number for this configuration, L = 1, is the same as if there were only one electron in the 5p subshell. Four of the five electrons in the 5p subshell are paired; with one unpaired electron, the spin quantum number, S, is 1/2. The term symbol for the ground state is written as $^2S + 1_L$ or ^2P. Because of the magnetic interactions of the electron spins with their orbital motion, the ^2P term is split into two spin orbit states corresponding to J = L + S and J = L - S where J is the total angular momentum quantum number. These fine structure components of the ^2P term are designated as $^2P_{1/2}$ and $^2P_{3/2}$ corresponding to J = L - S and J = L + S. The lowest energy state (ground state) is the $P_{3/2}$ state with the $^2P_{1/2}$ state being the first excited state. Following Hund's rule, the J = 3/2 state is lower in energy than the J = 1/2 state for the more than half filled subshell (Ref. 10). If the energy of the $^2P_{3/2}$ state is defined as zero, the $^2P_{1/2}$ state is at 0.9427 eV or 7602.9768 cm^{-1} (Ref. 11).

TABLE 3. Atomic iodine number density, N(I) in atoms/cm^3.

Total Pressure (torr)	Temperature (K) 473	732	794	823
0.372	7.97×10^{12}	4.83×10^{14}	9.05×10^{14}	1.29×10^{15}
0.831	1.19×10^{13}	7.34×10^{14}	1.40×10^{15}	2.02×10^{15}
1.76	1.73×10^{13}	1.08×10^{15}	2.08×10^{15}	3.05×10^{15}
3.56	2.47×10^{13}	1.55×10^{15}	3.02×10^{15}	4.44×10^{15}
6.88	3.43×10^{13}	2.16×10^{15}	4.24×10^{15}	6.27×10^{15}
12.8	4.68×10^{13}	2.96×10^{15}	5.82×10^{15}	8.64×10^{15}
22.9	6.25×10^{13}	3.97×10^{15}	7.82×10^{15}	1.16×10^{16}
39.7	8.23×10^{13}	5.22×10^{15}	1.03×10^{16}	1.54×10^{16}
66.7	1.07×10^{14}	6.78×10^{15}	1.34×10^{16}	2.01×10^{16}

Total Pressure (torr)	Temperature (K) 848	873	898	973
0.372	1.55×10^{15}	1.96×10^{15}	2.11×10^{15}	3.04×10^{15}
0.831	2.50×10^{15}	3.26×10^{15}	3.56×10^{15}	5.84×10^{15}
1.76	3.82×10^{15}	5.08×10^{15}	5.61×10^{15}	1.02×10^{16}
3.56	5.60×10^{15}	7.55×10^{15}	8.41×10^{15}	1.64×10^{16}
6.88	7.95×10^{15}	1.08×10^{16}	1.21×10^{16}	2.48×10^{16}
12.8	1.10×10^{16}	1.51×10^{16}	1.69×10^{16}	3.59×10^{16}
22.9	1.49×10^{16}	2.04×10^{16}	2.30×10^{16}	5.01×10^{16}
39.7	1.97×10^{16}	2.72×10^{16}	3.06×10^{16}	6.80×10^{16}
66.7	2.57×10^{16}	3.55×10^{16}	4.00×10^{16}	9.01×10^{16}

The total angular momentum of the iodine nucleus, or nuclear spin, is I = 5/2. This gives rise to a magnetic dipole moment of 2.81327 nuclear magnetons for the nucleus. There is also an electric quadrupole moment as a result of the nonspherical charge distribution in the nucleus. The accepted value for the electric quadrupole moment of the iodine nucleus is -0.789 barns (Ref. 12). Hyperfine structure in atoms arises from the interaction of electronic angular momentum and the angular momentum of the nucleus. The total angular momentum of the atom is given by coupling the orbital and nuclear angular momentum F = J + I, where the quantum number F can have the values

$$F = I + J,\ I + J - 1,\ I + J - 2\ ,\ \ldots\ |I - J| \tag{28}$$

The $^2P_{3/2}$ ground state splits into four hyperfine levels with F = 1, 2, 3 and 4. The $^2P_{1/2}$ excited state splits into two levels with F = 3 and 2. The splitting of the ^2P term into the $^2P_{3/2}$ and $^2P_{1/2}$ states and the hyperfine splitting are shown in Fig. 1. The energies of the hyperfine levels are given by

$$T_F = T_o + \frac{AC}{2} + \frac{B[3C(C+1)-4I(I+1)J(J+1)]}{8I(2I-1)J(2J-1)} \tag{29}$$

where

$C = F(F+1) - I(I+1) - J(J+1)$

$A = 27.59 \times 10^{-3}$ cm^{-1} (or 3.42×10^{-6} eV) for J = 3/2

$A = 219.73 \times 10^{-3}$ cm^{-1} (or 2.72×10^{-5}eV) for J = 1/2

$B = 38.12 \times 10^{-3}$ cm^{-1} (or 4.73×10^{-6}eV) for J = 3/2

B = 0 for J = 1/2

T_o = 0 for J = 3/2

T_o = 7602.9768 cm^{-1} (or 0.94266 eV) for J = 1/2

A is the nuclear magnetic dipole interaction constant,
B is the nuclear electric quadrupole interaction constant and T_o is the energy of the level in the absence of the hyperfine interaction (Ref. 11).

An electric dipole transition between the $^2P_{1/2}$ and $^2P_{3/2}$ states is forbidden since both states are of odd parity, L = 1. The selection rules for magnetic

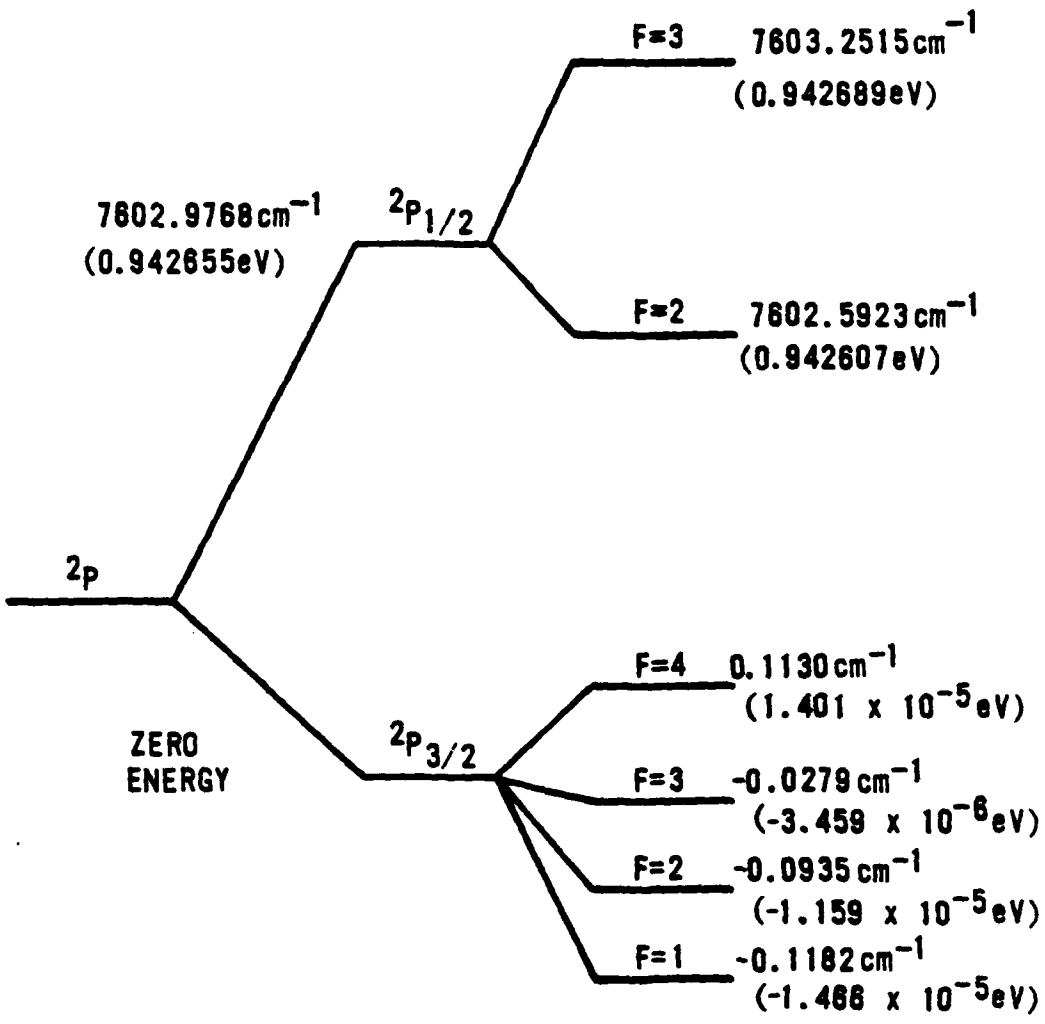

Figure 1. Energy level splitting of the ^2P term of atomic iodine.

dipole transitions are $\Delta L = 0$ and $\Delta J = 0, \pm 1$. For a transition from $^2P_{1/2}$ to $^2P_{3/2}$, $\Delta L = 0$ and $\Delta J = +1$; the magnetic dipole transition is allowed. The selection rule for transitions between hyperfine levels is $\Delta F = 0, \pm 1$ with $F = 0$ to $F' = 0$ excluded. A high resolution ($\lambda/\Delta\lambda$ on the order of 10^6) spectrum of the hyperfine structure in the $^2P_{1/2}$ to $^2P_{3/2}$ transition is shown in Fig. 2 (Ref. 11). The spectrum is divided into two groups of three peaks called triplets, corresponding to the allowed transitions from the $F = 3$ and $F = 2$ levels of the $^2P_{1/2}$ state. The $F = 3$ to 4 transition is easily the most intense and is the lasing transition of the atomic iodine lasers.

The intensities of the hyperfine transitions are related to the spontaneous emission probabilities, also known as the Einstein A coefficients. The natural or unperturbed lifetime of a transition is simply the reciprocal of the A coefficient. Spontaneous emission probabilities for the magnetic dipole transitions are given in Table 4 (Ref. 13). The $F = 3$ to 4 transition has the highest spontaneous emission probability and, therefore, the shortest lifetime of the hyperfine transitions. As discussed in the following paragraphs, the spontaneous emission probability is not the only factor in determining the intensities of transitions, but a comparison of the hyperfine transition intensities in Fig. 2 with the corresponding spontaneous emission probabilities in Table 4 shows a rough correlation.

The population of the hyperfine levels is another factor which determines the transition intensities. Each hyperfine level is $2F + 1$ fold degenerate with respect to the magnetic quantum number M_F. Since the energy splitting between hyperfine levels is small compared to kT, the population of the hyperfine levels is proportional to the statistical weights of the levels. In the $^2P_{1/2}$ state, the $F = 3$ level has a degeneracy of 7 and the $F = 2$ has a degeneracy of 5, so that the total degeneracy of the state is 12. Therefore, the statistical weight of the $F = 3$ level is 7/12. The total degeneracy of the $^2P_{3/2}$ state is 24 and the statistical weight of the $F = 4$ level is 9/24.

The relationship between the spontaneous emission probability, the degeneracies of the hyperfine levels, and absorption and emission is contained in the laser gain equation

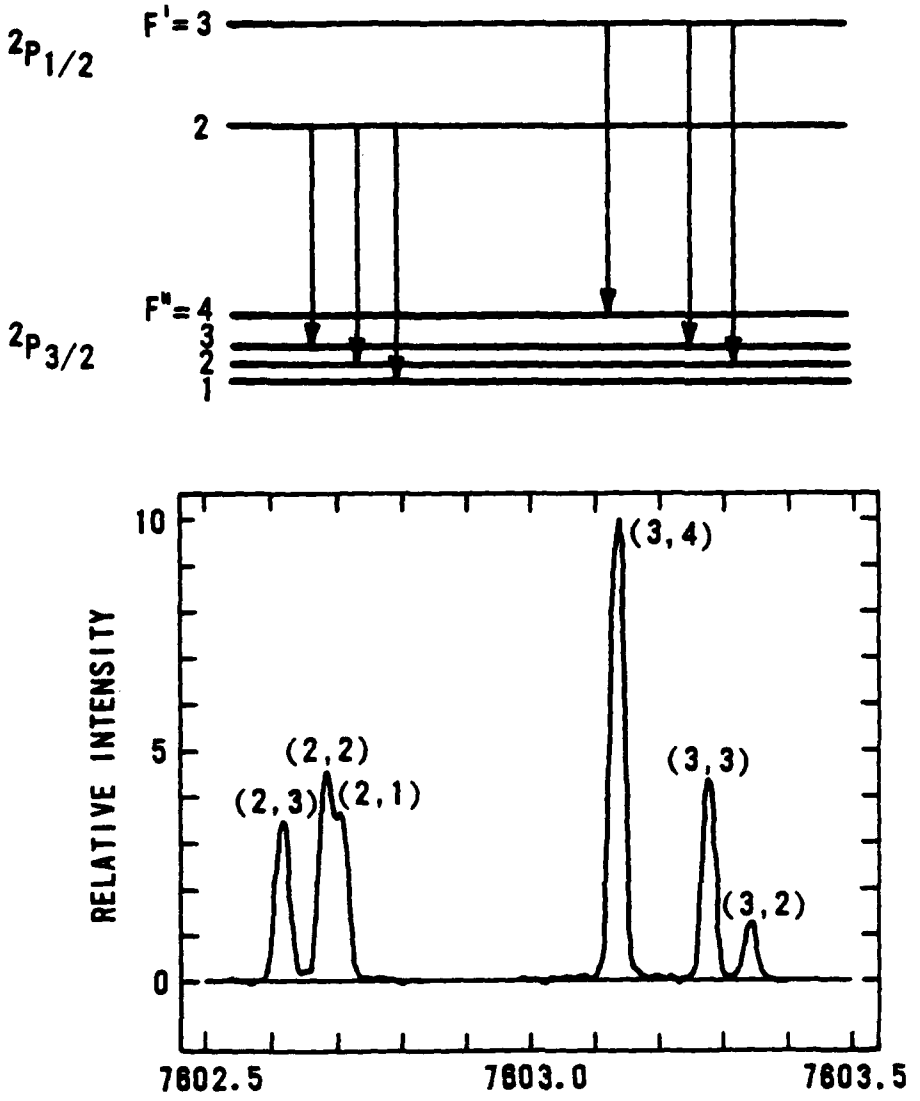

Figure 2. Hyperfine spectrum of the atomic iodine transition (cm^{-1}) (Ref. 11).

TABLE 4. Spontaneous emission probabilities for hyperfine transitions between the $^2P_{1/2}$ and $^2P_{3/2}$ states (Ref. 13).

Hyperfine Transition $F(^2P_{1/2})$ to $F(^2P_{3/2})$	Spontaneous Emission Probability (s^{-1})
3 - 4	5.0
3 - 3	2.1
3 - 2	0.6
2 - 3	2.4
2 - 2	3.0
2 - 1	2.3

$$G = \frac{A\lambda^2}{8\pi} \; g(\nu)[N_u - (g_u/g_L)N_L] \tag{30}$$

Here A = 5.0 s^{-1} (Ref. 13) and is the spontaneous emission rate for the F = 3 to 4 transition in iodine and λ is the transition wavelength (1.315×10^{-6}m). The magnitude of the lineshape function on resonance, $g(\nu)$, is given by

$$g(\nu) = \lambda \left(\frac{M_I}{2\pi kT}\right)^{\frac{1}{2}} \tag{31}$$

Here N_u is the number density in the upper level and is equal to 7/12 of the total number of iodine atoms in the $^2P_{1/2}$ state, N_{Iu}. The factor N_L is the number density in the lower level and is equal to 9/24 of the total number of iodine atoms in the $^2P_{3/2}$ state, N_{IL}. The degeneracy of the upper level, g_u, is 7 and the lower level degeneracy, g_L, is 9. Substituting these values into Eq. 30 gives

$$G = \frac{7}{12} \; \frac{\lambda^3 A}{8\pi} \left(\frac{M_I}{2\pi kT}\right)^{\frac{1}{2}} [N_{Iu} - \tfrac{1}{2}N_{IL}] \tag{32}$$

The quantity outside of the brackets is equal to σ, the stimulated emission cross section. If the iodine atoms are produced by thermal dissociation of I_2, nearly all will be in the ground state and N_{Iu} will be negligible. Equation 32 for this case becomes

$$G = \frac{-\sigma}{2} N(I) \tag{33}$$

since N_{IL} is now the total number density of iodine atoms, N(I), and G is the absorption per centimeter. Table 5 gives the absorption in percent per centimeter calculated from the values of N(I) in Table 3. The accuracy of these theoretical absorption values depends upon the accuracy of the assumed value of the A coefficient as well as that of the model used to calculate the values of N(I).

2.3 THE ZEEMAN EFFECT IN THE HYPERFINE LEVELS OF IODINE

An atom in free space has no preferred orientation in the absence of external fields.

TABLE 5. Calculated absorption in units of percent/cm at 1.315 μm.

Total Pressure (torr)	Temperature (K)							
	473	732	794	823	848	873	898	983
0.372	0.0024	0.116	0.209	0.290	0.346	0.432	0.459	0.634
0.831	0.0036	0.177	0.323	0.458	0.559	0.718	0.774	1.218
1.76	0.0052	0.260	0.480	0.692	0.853	1.119	1.218	2.127
3.56	0.0074	0.373	0.697	1.007	1.251	1.662	1.825	3.421
6.88	0.0103	0.519	0.979	1.422	1.776	2.378	2.627	5.173
12.8	0.0140	0.712	1.344	1.959	2.458	3.325	3.669	7.488
22.9	0.0187	0.955	1.806	2.631	3.329	4.492	4.989	10.45
39.7	0.0246	1.255	2.378	3.492	4.401	5.989	6.646	14.18
66.7	0.0320	1.630	3.094	4.558	5.742	7.817	8.689	18.79

The 2F + 1 fold degeneracy of the hyperfine levels is a result of this orientational independence. Eigenvalues of the z component of the total angular momentum are denoted by the magnetic quantum number M_F. Since there is no preferred direction for the z axis, the energies associated with the different values of M_F must all be the same. If the atom is placed in a magnetic field, however, the orientation of the atom with respect to field's direction becomes important. A preferred direction is established since the atoms will tend to orient themselves in the direction of lowest interaction energy. If the magnetic field is taken to be in the z direction with a magnitude of B_Z, the interaction of the atom with the field is given by

$$H' = \frac{2\pi\mu_B}{h} B_z (L_z + 2S_z) - g_I \left(\frac{2\pi\mu_N}{h}\right) B_z I_z \tag{34}$$

where μ_B is the Bohr magneton

$$\mu_B = \frac{eh}{4\pi m_{electron}} = 9.27408 \times 10^{-24} \text{ J/T} \tag{35}$$

μ_N is the nuclear magneton

$$\mu_N = \frac{eh}{4\pi m_{proton}} = 5.05082 \times 10^{-27} \text{ J/T} \tag{36}$$

g_I is the nuclear g factor, and I_z is the z component of the nuclear spin. The second term on the right in Eq. 34 is the interaction of the nuclear magnetic moment with the field and can be neglected in most cases (Refs. 3 and 10). The factors, L_z and S_z, in Eq. 34 are the z components of the orbital and spin angular momentum, respectively. The method of treating the interaction depends upon the strength of the magnetic field and the magnitude of the hyperfine splitting. This work deals only with cases in which the interaction of the atom with the magnetic field is less than the hyperfine interaction. However, a brief mention of the effects of higher field strengths is appropriate. If the magnetic field interaction is greater than the hyperfine interaction, the hyperfine interaction can be treated as a perturbation. The strong field uncouples the interaction between the nuclear spin, I, and the total angular momentum of the electrons, J. The nuclear spin is split into 2I + 1 components and the total angular momentum of the electrons is split into 2J + 1 components. In cases where the magnetic field interaction

is on the same order of strength as the hyperfine interaction, I and J are once again coupled; $M_F = M_I + M_J$ and $F = I + J$. In these cases, the hyperfine and magnetic field interactions are treated equally.

For the magnetic field strengths used in this work, the hyperfine splitting is much greater than the Zeeman splitting of the hyperfine levels. Accordingly, the magnetic field interaction is treated as a perturbation and the shifted energy levels are given by

$$E(F,M_F) = T_F + g_F \mu_B B_z M_F \tag{37}$$

where T_F is the energy of the F^{th} hyperfine level (Eq. 29) and g_F is the Landé factor given by

$$g_F = g_J \frac{[F(F+1) - J(J+1) - I(I+I)]}{2F(F+1)} \tag{38}$$

Here g_J is the Landé factor in the absence of a nuclear magnetic moment:

$$g_J = 1 + \frac{[J(J+1) + S(S+1) - L(L+1)]}{2J(J+1)} \tag{39}$$

Note that from Eq. 37 the energy shift is proportional to the magnetic field strength. Each hyperfine level will be split into 2F + 1 equally spaced components designated by the quantum number M_F. This model for the upper and lower levels in the iodine laser transition is good for fields up to 1000 gauss (0.1 T). Figures 3 and 4 show the calculated splitting of the $^2P_{1/2}$ F = 3 and $^2P_{3/2}$ F = 4 levels of iodine as functions of the magnetic field using Eq. 37. Note that the splitting in the $^2P_{1/2}$ F = 3 level is much less than the splitting in the $^2P_{3/2}$ F = 4 level.

The selection rules for transitions between magnetic hyperfine levels in the presence of a weak magnetic field are $\Delta F = 0, \pm 1$ and $\Delta M_F = 0, \pm 1$. The lasing transition is split into 21 components since there are three allowed transitions from each of the seven M_F levels in the upper state to the nine M_F levels in the lower state. Transitions between the magnetic hyperfine levels have a definite polarization in the presence of a magnetic field. A transition between levels where $\Delta M_F = \pm 1$ is called a π transition and is associated

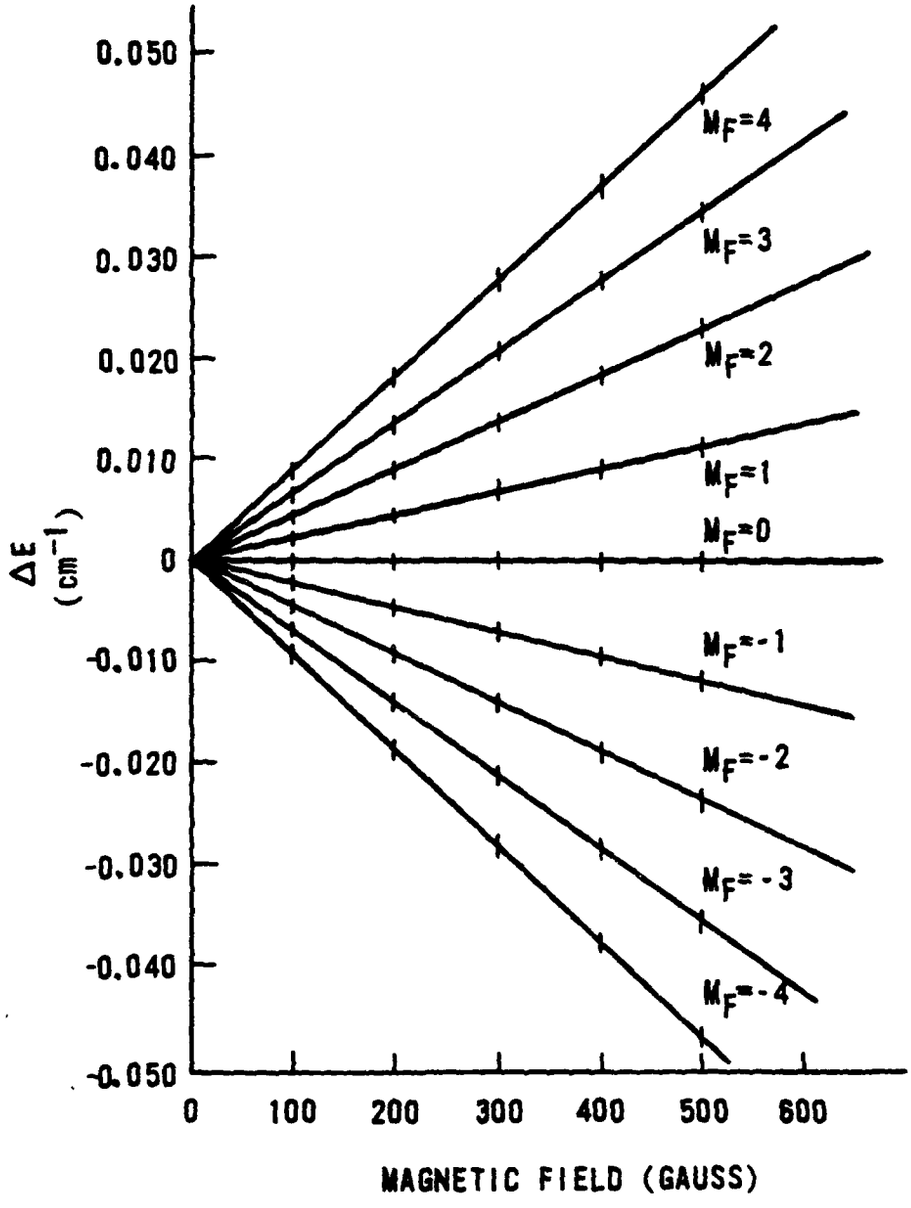

Figure 3. Magnetic hyperfine splitting of the $^2P_{3/2}$ F = 4 level.

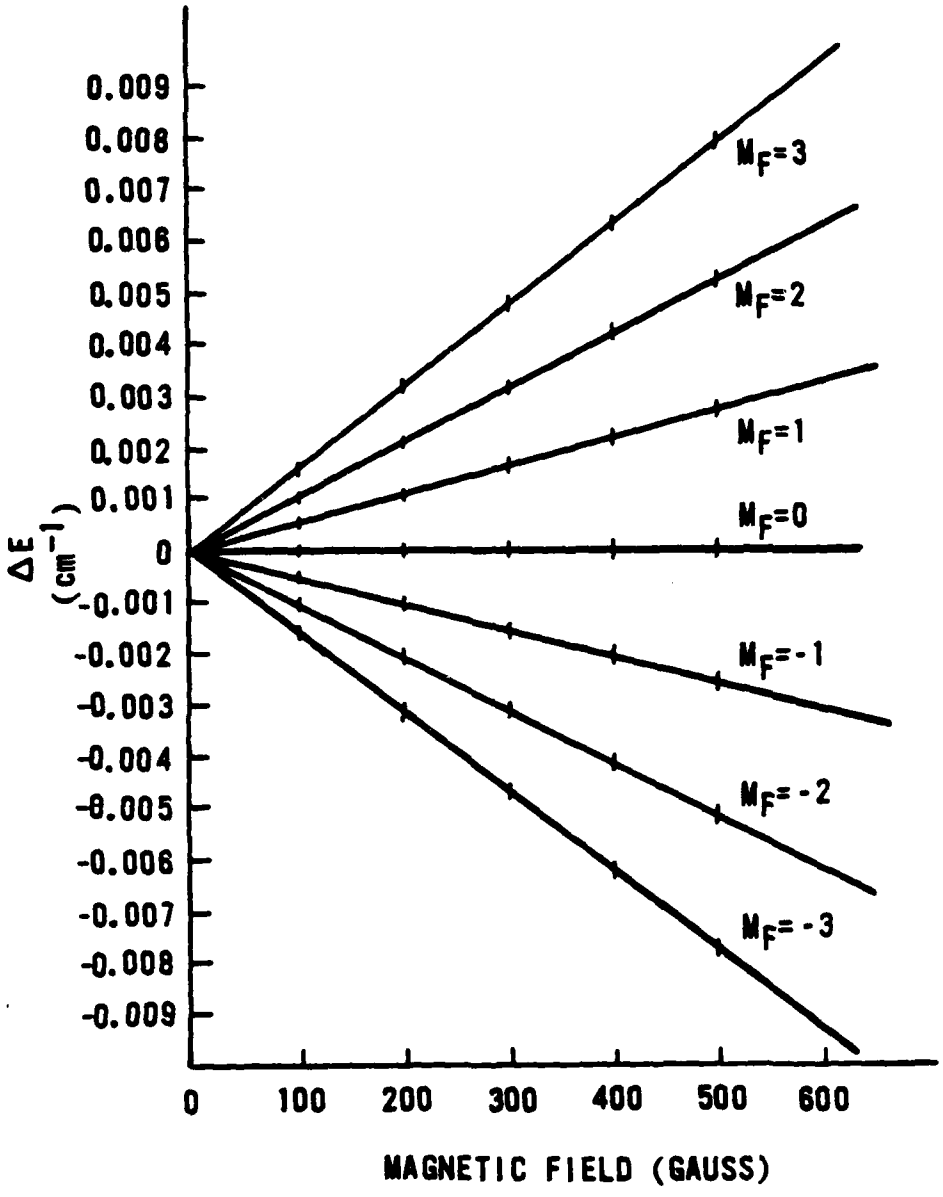

Figure 4. Magnetic hyperfine splitting of the $^2P_{1/2}$ F = 3 level.

with radiation polarized parallel to a field that is transverse to the direction of propagation. For transitions where $\Delta M_F = 0$, known as σ transitions, the radiation is polarized perpendicularly to the transverse magnetic field. If the magnetic field is parallel to the optical axis, the σ transitions do not occur and the π transition radiation is circularly polarized (Ref. 10).

In the presence of a magnetic field the gain or absorption for an individual magnetic hyperfine transition is given by

$$G_H = \frac{\lambda^2}{8\pi} g(\nu) A(M_{F3}, M_{F4})[N_{M_{F3}} - N_{M_{F4}}] \tag{40}$$

This equation is analogous to Eq. 30. The line-shape function, $g(\nu)$, is given by Eq. 31 and λ is the transition wavelength. The factor $A(M_{F3}, M_{F4})$ is the Einstein A coefficient for the magnetic hyperfine transition, and $N_{M_{F3}}$ and $N_{M_{F4}}$ are the number densities in the upper and lower magnetic hyperfine levels. If we assume that the populations of the magnetic hyperfine levels are equal within a given hyperfine level, then Eq. 40 becomes

$$G_H = \frac{\lambda^2 g(\nu)}{8\pi} A(M_{F3}, M_{F4}) \frac{1}{7} [N_u - (7/9)N_L] \tag{41}$$

where N_u and N_L are the number densities in the upper (F = 3) and lower (F = 4) hyperfine levels. The A coefficients for the allowed magnetic hyperfine transitions as calculated in Ref. 3 are listed in Table 6. From Eq. 41, we see that the strength of the transition depends on the A coefficient. The transitions with the largest A coefficients will have the highest absorption (or gain). The line positions and relative strengths of the σ and π components for the F = 3 to 4 transition in a magnetic field of 500 gauss are shown in Fig. 5 and the corresponding transition energies are listed in Table 6. For the conditions in this work, the σ transitions do not occur since the laser beam is parallel to the magnetic field. The $M_F = 0$ to 0 transition is the laser transition and there are no π transitions associated with it. If the transition line widths were infinitely narrow, any shift in the transition's energy would result in no absorption. However, the transitions have a finite line width. In the following discussion, this line width is calculated and the effects of pressure and temperature on it are explored.

TABLE 6. Magnetic hyperfine transition energies for a magnetic field of 500 gauss.

$M_F' \rightarrow M_F$	A Coefficient (ref.3)	Transition Energy (cm^{-1})	ΔE (cm^{-1})	ΔE (MHz)
3,4	3.990	7603.099602	-0.038898	-1166.13
3,3	0.959	7603.111272	-0.027228	- 816.274
3,2	0.240	7603.122942	-0.015558	- 466.416
2,3	2.997	7603.108678	-0.029822	- 894.040
2,2	1.680	7603.120348	-0.018152	- 544.182
2,1	0.479	7603.132018	-0.006482	- 194.325
1,2	2.157	7603.117754	-0.020746	-621.948
1,1	2.157	7603.129424	-0.009076	-272.091
1,0	0.959	7603.141094	.002594	+ 77.766
0,1	1.438	7603.126830	-0.011670	-349.857
0,0	1.199	7603.138500	0	0
0,-1	1.438	7603.150170	0.01167	349.857
-1,0	0.959	7603.135906	-0.002594	-77.7660
-1,-1	2.157	7603.147576	0.009076	272.091
-1,-2	2.157	7603.159246	0.020746	621.948
-2,-1	0.479	7603.144982	0.006482	194.325
-2,-2	1.680	7603.156652	0.018152	544.182
-2,-3	2.997	7603.168322	0.029822	894.040
-3,-2	0.240	7603.154058	0.015558	466.416
-3,-3	0.959	7603.165728	0.027228	816.274
-3,-4	3.990	7603.177398	0.038898	1166.13

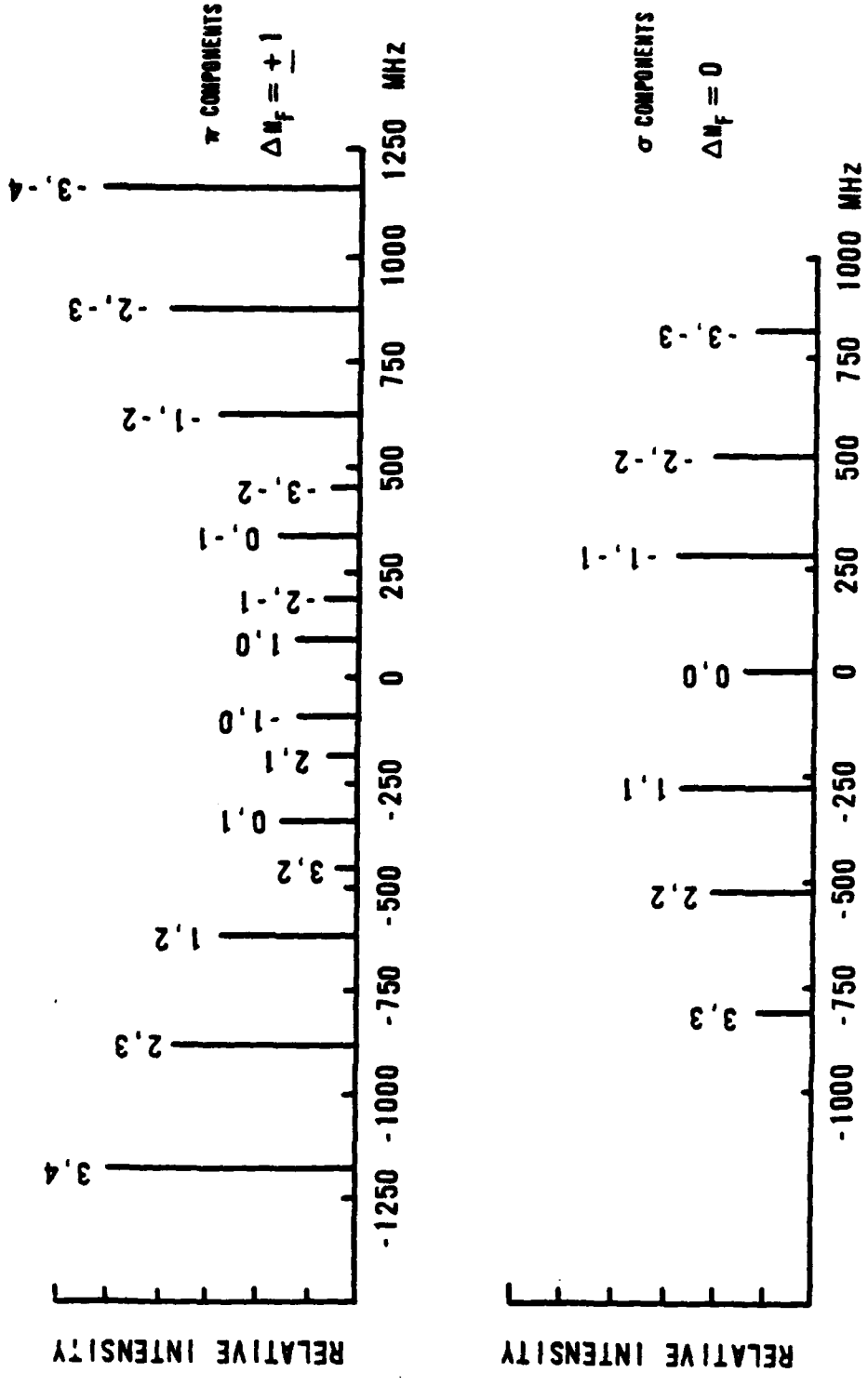

Figure 5. Computed line positions and relative strengths of the magnetic hyperfine transitions for a magnetic field strength of 500 gauss.

2.4 LINE WIDTHS

The natural Lorentzian line width, which arises from the uncertainty principle, is extremely small. The actual line width, however, is determined by pressure and temperature broadening effects.

Doppler broadening is associated with the shift in frequency of emitted or absorbed radiation because of the Doppler shift. Higher velocities result in a greater Doppler shift in the absorbed or emitted frequencies. The Doppler broadening of a spectral line is given by

$$\Delta\nu = \frac{2\nu_0}{c}\left[\frac{2kT(\ln 2)}{M_I}\right]^{\frac{1}{2}} \qquad (42)$$

For iodine at 300 K, the Doppler broadened line width is 251 MHz or 0.0086 cm^{-1}.

In a gas, iodine atoms collide with each other as well as other collision partners. These collisions can cause an atom in an excited state to make a radiationless transfer to a lower state, decreasing the lifetime of the excited state. In this work the principal collision partners present were iodine atoms and molecules. Oxygen and nitrogen may have been present as a result of leaks in the system but only in amounts which were much less than a torr, making the effect from these gases negligible. Pressure broadening coefficients for iodine atoms and molecules have been measured at 1000 K to to be 1.3 MHz/torr ($4.34 \times 10^{-5} cm^{-1}$/torr) for atomic iodine and 3.1 MHz/torr ($1.03 \times 10^{-4} cm^{-1}$/torr) for molecular iodine (Ref. 14).

The line-shape in the case of pure Doppler broadening is Gaussian, while the line-shape for pressure broadening only is Lorentzian. The true line-shape of a transition is a combination of the pressure broadened and Doppler broadened line-shapes. The Voigt profile is a good approximation of the true line-shape. It is obtained by combining a Gaussian profile with a Lorentzian function in the form of a folding integral using a parameter (η) which describes the relative weights of the Gaussian and Lorentzian functions. The half width at half maximum for the Voigt Profile, $\delta/2$, has been tabulated

for values of the parameter η ranging from 0.1 to 10.0 in Ref. 15. The parameter η is given by

$$\eta = \frac{\Delta\nu_D}{\Delta\nu_p(\ln 2)^{\frac{1}{2}}} \tag{43}$$

where $\Delta\nu_D$ is the Doppler line width obtained from Eq. 42, $\Delta\nu_p$ is the pressure broadened line width obtained by a simple sum of the line widths because of I_2 pressure broadening and atomic iodine pressure broadening using the pressure broadening coefficients from Ref. 14. The Voigt line width is then given by

$$\Delta\nu_V = \frac{\delta}{\eta} \quad \frac{\Delta\nu_D}{2(\ln 2)^{\frac{1}{2}}} \tag{44}$$

where $\delta/2$ is obtained from Table 1 in Ref. 15. For $\eta = 10.0$ (the maximum value in Table 1), the pressure broadening is small and the Doppler line-width is 94 percent of the Voigt line width. For iodine pressures < 20 torr, pressure broadening effects are negligible and the Doppler line-width accounts for more than 94 percent of the Voigt line width. Calculated line widths for the iodine laser transition are listed in Table 7. The values given for the Doppler broadened line widths, $\Delta\nu_D$, were calculated from Eq. 42 and are good approximations of the total line widths at pressures < 20 torr. The line widths calculated for a pressure of 66.7 torr are the Voigt line widths from Eq. 44. In this case, Eq. 43 and the values for $\Delta\nu_D$ and $\Delta\nu_p$ were used to calculate η. The percent dissociation given in the last column was used to determine partial pressures in the gas. For example, at 898 K the gas composition was 80 percent iodine atoms and 20 percent iodine molecules (Ref. 8).

2.5 ABSORPTION SUPPRESSION

Reexamining Fig. 5 in light of the line widths in Table 7, absorption at the $M_F = 0$ to 0 transition energy for the π components is not reduced to zero in the presence of a magnetic field, but will have some nonzero value because of overlapping contributions from the adjacent transitions. As the magnetic

TABLE 7. Line widths for the iodine laser transition.

Temperature	$\Delta\nu_D$		$\Delta\nu_p$	n	$\delta/2$ (Ref. 15)	$\Delta\nu_V$(66.7 torr)		% Dissociation (Ref. 8)
(K)	(MHz)	(cm^{-1})	(MHz)			(MHz)	(cm^{-1})	
473	315	0.0105	206	1.84	2.118	436	0.0145	0%
732	392	0.0131	186	2.53	2.667	496	0.0165	17.8%
794	408	0.0136	164	2.99	3.067[a]	503	0.0168	36.1%
823	416	0.0139	147	3.40	3.403[a]	499	0.0166	50.4%
848	422	0.0141	135	3.75	3.691[a]	499	0.0166	60.5%
873	428	0.0143	120	4.28	4.128[a]	496	0.0165	72.1%
898	434	0.0145	111	4.70	4.474[a]	496	0.0165	80.0%
973	452	0.0151	86.7	6.26	5.766[a]	500	0.0167	~100 %

Note: [a] values were interpolated from Table 1 in Ref. 15.

field strength is reduced, the extent of the energy level splitting decreases, and the line width overlap at the laser transition energy increases, as well as the absorption. For zero magnetic field strength, the magnetic hyperfine energy levels are degenerate and the absorption of the laser radiation is at a maximum.

A quantitative theoretical evaluation of the absorption magnetic field relation was not within the scope of this work. The qualitative discussion presented here is sufficient for evaluating the data presented in the fourth section.

3.0 EXPERIMENTAL APPARATUS

3.1 ATOMIC IODINE LASER

The C_3F_7I photodissociation laser which was used as the source of 1.315 μm radiation was developed and built at the Air Force Weapons Laboratory (AFWL) and is briefly described here (Ref. 16). A mercury arc lamp enclosed in a water cooled coaxial quartz jacket was operated at 2400 W, providing ultraviolet light which photolyzed C_3F_7I producing excited iodine atoms. The cooling water was circulated through a deionizer to remove metallic impurities which would otherwise form an opaque coating on the outside of the lamp. A water resistivity of 12 MΩ-cm was typical. Ultraviolet radiation from the arc lamp was focused along the optical axis by placing the lamp at one focus of a polished aluminum reflector (which was in the shape of an elliptical cylinder) and the optical axis of the laser at the other focus. The reflector housing was also water cooled.

The C_3F_7I supply system is shown in Fig. 6, and a detailed description can be found in Ref. 17. This closed-cycle system provided a continuous supply of gaseous C_3F_7I at fixed pressure and flow velocity. The heart of the system is the condenser-evaporator unit. Denatured alcohol cooled to -55°C flowed through a helical coil in the condenser cell. At this temperature, the vapor pressure of the liquid C_3F_7I is 5.8 torr. Impurities such as I_2 or H_2O have negligible vapor pressures at -55°C and remained frozen in the condenser cell. The condenser cell was connected to the evaporator cell by a 0.6 cm ($\frac{1}{4}$ in) diameter glass tube near the bottom of both cells. A cooling jacket with denatured alcohol cooled to -20°C flowing through it surrounded the evaporator cell. At -20°C the vapor pressure of C_3F_7I is 53 torr. The pressure differential between the two cells produced flowing C_3F_7I gas. The flow velocity depended on the various constrictions in the system and the temperature and pressure differentials between the condenser and the evaporator. During operation of the laser, the flow velocity of the fuel through the cavity was 1 to 2 m/s (Ref. 18).

The C_3F_7I laser fuel was purchased * as 99 percent pure N-Heptafluoropropyl Iodide. A fractional distillation procedure was used to further purify the

*Columbia Organic Chemicals Co, Inc,
Camden, SC 29020

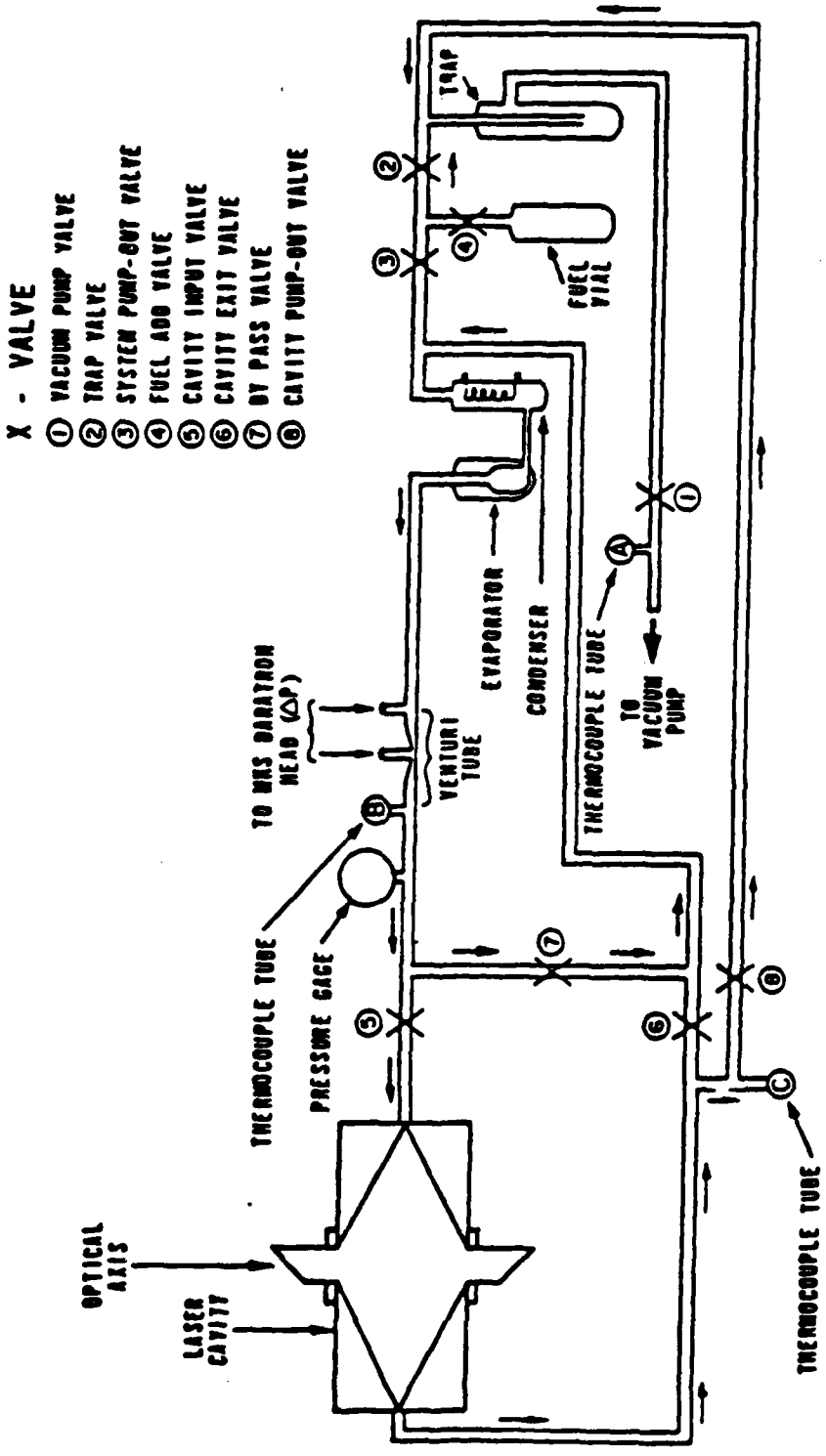

Figure 6. C_3F_7I supply system.

laser fuel (Ref. 19). Approximately 100 ml of purified C_3F_7I were poured into the fuel vial which was then attached to the supply system and frozen in liquid nitrogen (LN_2). The fuel add valve was then opened, and frozen air was pumped out of the fuel vial. At LN_2 temperatures (-196°C), C_3F_7I has a vapor pressure of $< 10^{-4}$ torr whereas oxygen and nitrogen at this temperature have vapor pressures of 100 and 600 torr, respectively. Pumping the entire system down to 0.10 to 0.20 torr reduced the air impurities to negligible levels. It was important to keep oxygen out of the system because oxygen causes rapid loss of excited atomic iodine through the resonant energy transfer process (Ref. 20).

$$I(^2P_{1/2}) + O_2(^3\Sigma) \rightarrow I(^2P_{3/2}) + O_2(^1\Delta_g) \qquad (45)$$

After fuel was loaded into the system, the trap valve, cavity input valve, and cavity exit valve were closed. The fuel vial was immersed in room temperature tap water causing it to vaporize into the system and condense in the condenser. Once all the fuel had evaporated from the fuel vial, the fuel add valve was closed as were the system pump-out valve, cavity pump-out valve, and cavity by-pass valve. The cavity input valve and cavity exit valve were then opened. The trap was immersed in LN_2 and the system was pumped down to a pressure of 15 to 20 torr by opening the system pump-out valve and the trap valve. Thus, the LN_2 cold trap collected any excess fuel for reuse. Operating in the 15 to 20 torr pressure range gave the most stable output from the laser. An atmospheric leak rate of 0.350 torr/h necessitated pumping down the system periodically to keep air impurities from having a significant effect on the laser output.

A schematic of the laser cavity and optical system is shown in Fig. 7. The gain length was 10 cm and consisted of the expanded area in the center of the flow channel where the ultraviolet light from the arc lamp was focused onto the laser fuel. Fused silica windows, mounted at Brewster's angle, were located at both ends of the laser cavity. Although the windows were removed from the flow channel, iodine would accumulate on the window overnight if the cavity was not thoroughly evacuated and isolated from the fuel supply system. The laser mirrors were both 5-cm-dia fused silica substrates, coated for maximum reflectivity (99.5 percent) at 1.315 μm. One mirror was a maximum

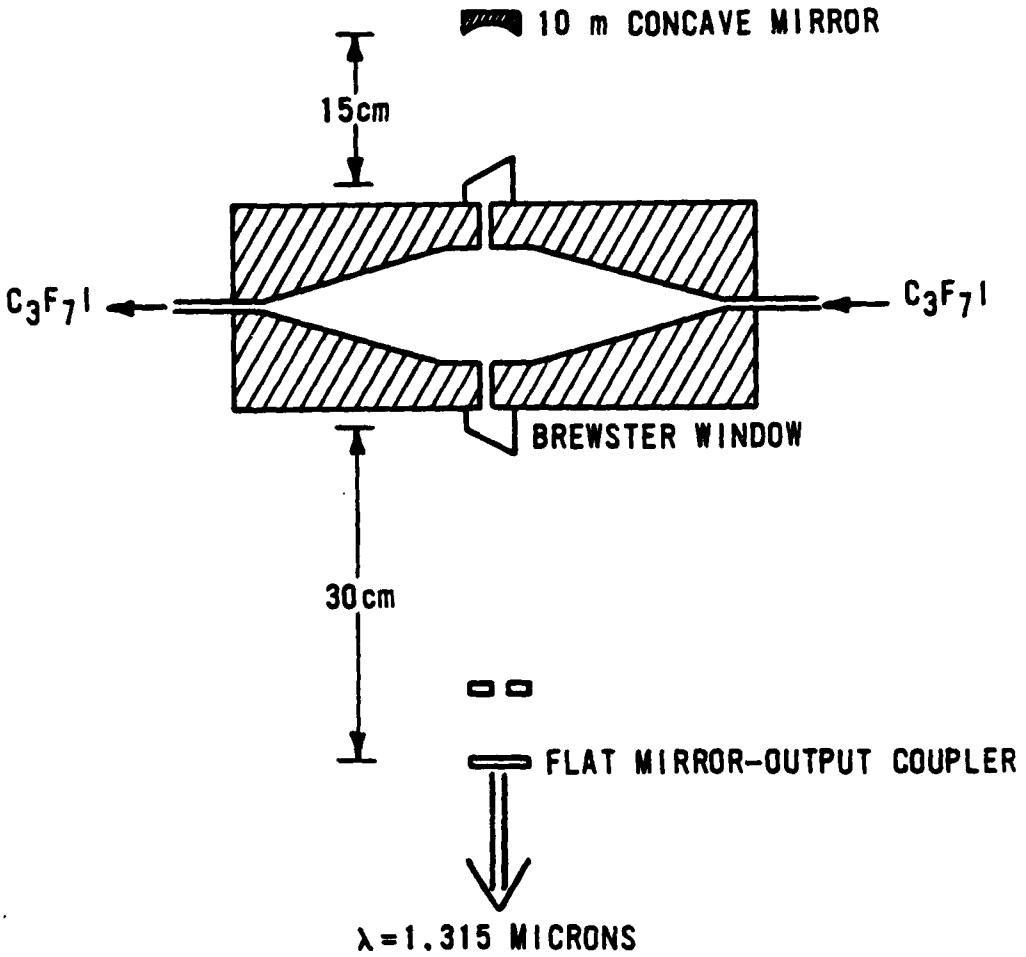

Figure 7. Laser cavity and optical system.

reflector with a radius of curvature of 10 m and the other was flat and served as the outcoupler. The total length of the optical cavity was 64 cm from one mirror to the other. An iris of variable radius was placed intracavity, 5 cm from the outcoupler. Without the iris, or when the iris was opened more than a centimeter, a number of transverse modes were observed using a Kodak IR phosphor card. Constant shifting from one mode to another caused unacceptable instability in the signal. Closing the iris to a diameter of ~ 3 mm eliminated all modes except the TEM_{00} mode which greatly increased signal stability. Radiation from the laser was directed through the absorption cell.

3.2 HEATED ABSORPTION CELL AND IODINE SUPPLY SYSTEM

Figure 8 is a schematic diagram of the heated absorption cell used in this experiment. The cell was made of 2.54-cm-dia fused silica tubing. The windows were cut from 5-cm-dia, 1-cm-thick fused silica flats and were laser welded at Brewster's angle to the 2.54 cm tubing with a CO_2 laser. The tubing extended 2.54 cm beyond the window allowing the heating elements to cover the entire active volume of the cell, thus, minimizing any cooling at the ends of the cell. A 0.64 cm fused silica tube attached to the side of the cell led to a sidearm containing iodine crystals. The absorption cell and sidearm are shown in Fig. 9 along with the heating and temperature measurement apparatus. An MKS* Model 315 bakeable pressure sensor head was attached to a 0.64 cm fused silica tube with a 0.64 cm (¼ in) ultratorr fitting and viton o-rings. A 1.3 cm (½ in) Kontes** Hi Vacuum Teflon valve with viton o-rings was used to isolate the system from a Varian*** HSA 2 in (5 cm) diffusion pump. The valve and the ultratorr fitting were the weak links in this otherwise sealed fused silica system.

Three Omega**** Model 4001 digital temperature controllers, capable of maintaining the set-point temperature to ±1°C, were used to maintain the desired temperatures in the three sections of the system. Omega high temperature

---

* MKS Instruments, Burlington, MA 01803
Kontes Glass Co., Vineland, NJ 08360
Varian Associates, Palo Alto, CA 94303
Omega Engrg, Inc., Stamford, CT 06907

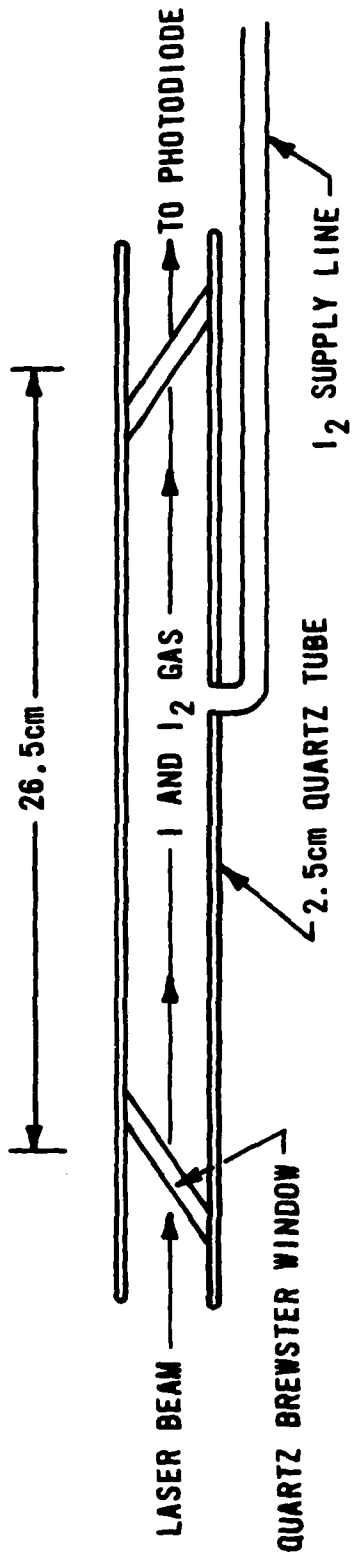

Figure 8. Absorption cell.

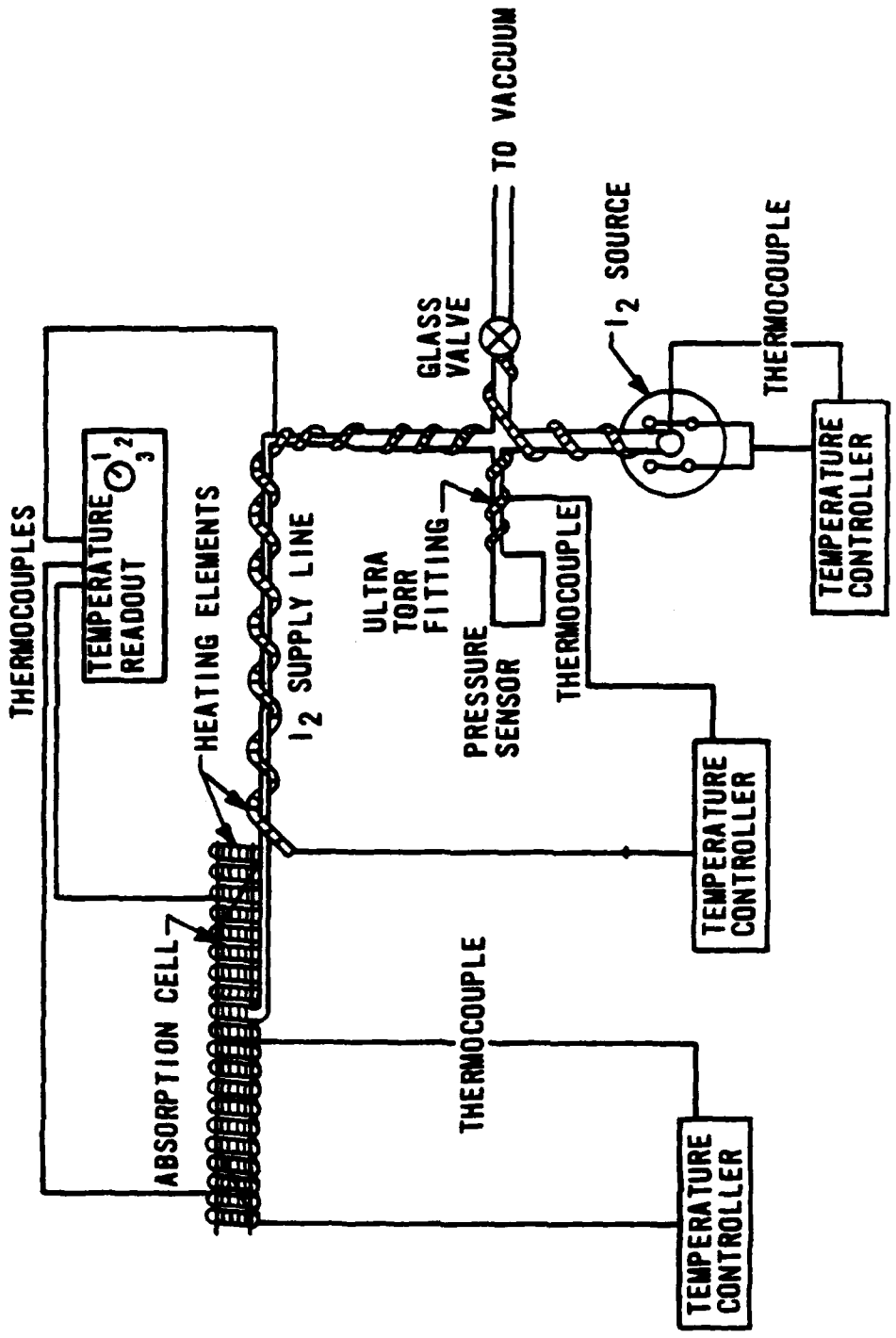

Figure 9. Absorption cell, supply line and I_2 source with heating set-up.

Chromel-Alumel thermocouples (type K) were placed in contact with the fused silica at three points on the absorption cell and at two locations on the supply line. The thermocouple placed at the midpoint of the absorption cell was connected to a temperature controller. The other two thermocouples at the ends of the absorption cell were connected to an Omega Model DSS-199 digital thermometer. Another thermocouple, located at the right angle bend in the supply line, was also connected to the digital thermometer. The controlling temperature of the supply line was monitored by a thermocouple located at the junction of the 0.64 cm (¼ in) ultratorr fitting and the 0.53 cm (¼ in) fused silica tube leading to the pressure sensor. The temperature of the supply line needed to be higher than the temperature of the iodine source, since the vapor pressure of iodine in the system was determined by the lowest temperature in the system. However, the Viton o-rings (used in the ultratorr fitting and valve) decompose in the presence of iodine at temperatures above 200°C. By controlling the temperature at the fitting, a safe operating temperature was maintained.

The iodine source for the absorption cell is shown in Fig. 10. The fused silica tube containing the iodine crystals fit snugly inside the brass heating block with < 0.124 cm clearance along the side. An Omega Chromel-Alumel thermocouple (type K) made of 0.025 cm (0.010 in) diameter wire was placed at the rounded end of the fused silica tube and connected to a temperature controller. Four Chromalox* CIR-1040 cartridge heaters fit into the 0.64 cm (¼ in) diameter holes in the brass heating block. They were connected in parallel to the temperature controller by way of a variable autotransformer, Statco Energy Products ** type 3PN1010. The output from the temperature controller was 7A at 120V. The transformers limited the power to the heating elements and permitted more control over the heating of the system.

The supply line and absorption cell were wrapped with NiChrome wire and insulated with 0.64 cm (¼ in) diameter ball and socket ceramic beads***. Separate wires and temperature controllers were used for the supply line and the absorption cell. Cartridge heaters, like those used to heat the iodine source tube, were placed at each end of the absorption cell to compensate for any

* Chromalox, Pittsburgh, PA 15212
Statco Energy Products, Dayton, OH
Cole-Parmer, Chicago, IL 60648

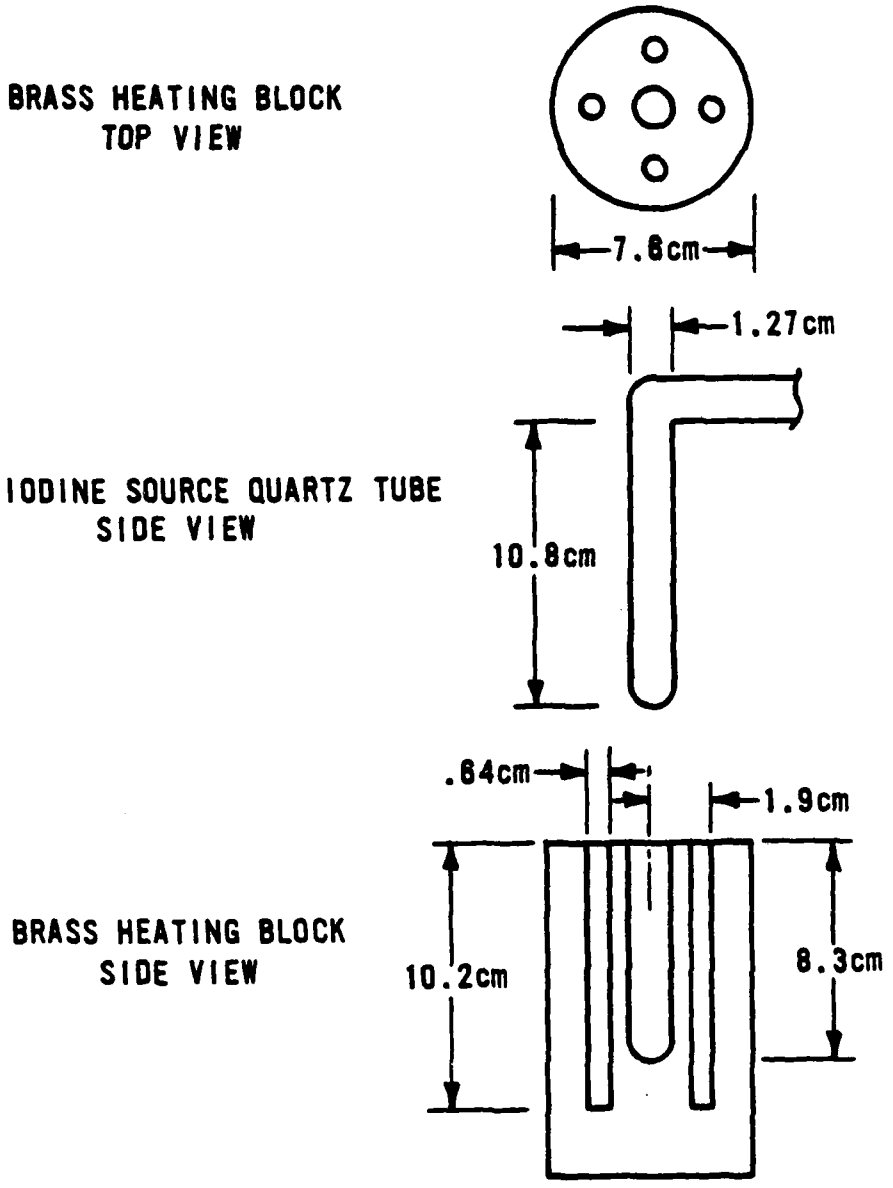

Figure 10. I_2 source system.

extra heat loss there. Variable autotransformers were used to control the power supplied to the heating wires. A 2.5-cm-thick layer of Cerablanket* insulation was wrapped around the absorption cell and heating wire. The three thermocouples were held in place by embedding them in the insulation, allowing only the tips to contact the quartz tube at the 0.64 cm (¼ in) spaces between the heating wires. The cell, heaters, thermocouples and insulation were then placed in a 7.6 cm (3 in) inside diameter copper pipe which acted as a form for the magnetic coil. This left some uncertainty about whether the thermocouples remained in contact with the fused silica tube and thus were a possible source of error in the measurement of the absorption cell temperature. The supply line was wrapped with a 1-cm-thick layer of Cerablanket insulation. The exact temperature of the supply line was not critical as long as it was warmer than the iodine source temperature and had no cold spots where the iodine could condense. Care was taken to ensure that all areas of the supply line were adequately heated and insulated. During normal operation, the supply line was kept at 100°C. The temperature of the MKS pressure sensor was maintained at 100°C by an MKS model 170M temperature controller/ compensator.

The entire system was initially attached to the diffusion pump and evacuated while the absorption cell was heated to 600°C (873 K), the supply line to 150°C, and the iodine source tube to 100°C. This bake-out took place over a period of 3 days for 8 h each day. During the evenings, the absorption cell and supply line were cooled to 100°C as a safety precaution. After this initial bake-out, the system was cooled to room temperature (25°C) and checked for leaks with a Varian model 936-40 helium leak detector. No leaks were found. The system was then isolated from the pump by closing the 0.64 cm (¼ in) glass valve. Over a period of 24 h, the pressure in the system, as monitored by the MKS pressure sensor, showed an atmospheric leak rate of ~ 0.001 torr per hour. When the absorption cell was heated to 200°C and the supply line was heated to 100°C, the leak rate rose dramatically to about 0.34 torr/h. Varying the iodine source tube temperature had no effect on the 0.34 torr/h leak rate. Heating the absorption cell to 500°C raised the leak

* Manville Refractory Products, Denver, CO 80217

rate to 0.48 torr/h. Raising the supply line temperature on the other hand had the largest effect, increasing the leak rate to 1.3 torr/h when its temperature was raised to 140°C. No leak could be found in the supply line with the helium leak detector, so outgassing was suspected. The o-rings in the valve and the ultratorr fitting were replaced with new Viton o-rings, but this had no effect on the leak rate. The decision was made to proceed and to take absorption data in spite of the leak. The iodine pressure in the cell was determined by the temperature of the iodine source tube. The pressure sensor measured the total pressure in the system, resulting from iodine vapor and whatever impurities had leaked or outgassed into the system. The temperature of the iodine source was known to ±3°C since the accuracy of the thermocouple and readout was ±3°C. At 27°C, this corresponds to an uncertainty in the iodine pressure of ±0.104 torr. At 67°C the uncertainty in the iodine vapor pressure was ±1.44 torr and it was even greater at higher temperatures. The temperature of the absorption cell on the other hand, was constant to within ±10°C across the length of the cell. This fact was established by measuring the temperature with a separate thermocouple which was situated between the heater and insulation and was moved from the edge to the center of the cell.

3.3 MAGNETIC COIL

The solenoidal coil used to create the magnetic fields in this experiment is shown in Fig. 11. A 50.8-cm-long copper pipe with a 7.6 cm (3 in) inside diameter and a 9.53 cm outside diameter acted as the form for the windings of 10 gauge polyester coated copper wire. The ends of the coil were insulated with 25.4-cm-dia, 2.54-cm-thick disks of G-10. The ends of the copper pipe were fitted with cooling water jackets as a precaution against the coil being damaged by the intense heat generated by the absorption cell heater. The coil was composed of three separate windings: a middle section 45.7-cm-long with a total of 2119 turns in 13 layers or 163 turns per layer, and two end sections which were each 15.2-cm-long with 432 total turns in 8 layers or 54 turns per layer. The three windings were wired together in series to a single power supply. The purpose of the end sections was to boost the magnetic field near the ends of the coil and keep the field uniform over the 26.5 cm region occupied by the absorption cell.

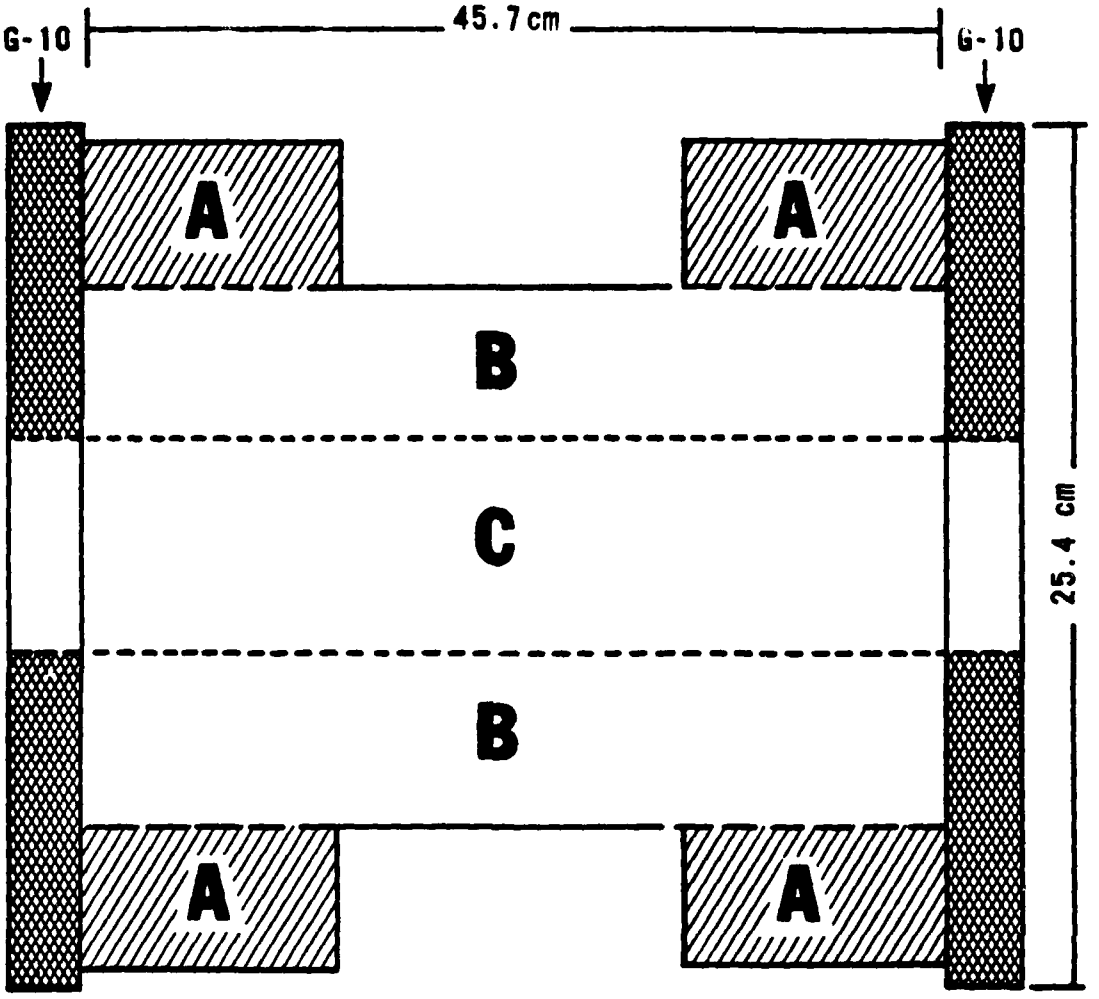

A. End section windings, 432 turns each.
B. Middle section windings, 2119 turns.
C. Hollow copper pipe, 7.6 cm I.D., 50.8-cm-long.

Figure 11. Magnetic coil.

The magnetic field strength inside the coil was calculated using the computer program presented in Appendix A, which is capable of calculating the magnetic field at any point inside or outside the coil. The z axis is taken to be along the center of the coil. Using cylindrical coordinates, the ρ axis is directed radially, perpendicular to the z axis. The coil is assumed to be symmetrical with respect to a plane passing through the center of the coil, perpendicular to the z axis of symmetry. The origin is defined to be at the intersection of this plane and the z axis. The program treats the coil as three sections: two end sections and a middle section. The coil length, the inner and outer diameters, the number of turns per layer, the total number of turns for each section, as well as the number and spacing of the calculation points along the z and ρ axis are the input parameters. The z component (B_z), ρ component (B_ρ), and the total magnetic field, $B_{tot} = [(B_z)^2 + (B_\rho)^2]^{1/2}$, are calculated at each point by calculating the contribution of each of the three loops in the coil to the field at that point and then summing the contributions. The components B_z and B_ρ at any point (z, ρ), relative to a current loop with its center at the origin, are given by

$$B_\rho = \frac{\mu I}{2\pi} \frac{z}{\rho[(a+\rho)^2+z^2]^{1/2}} \left[-K + \frac{a^2+\rho^2+z^2}{(a-\rho)^2+z^2} E\right] \tag{46}$$

and

$$B_z = \frac{\mu I}{2\pi} \frac{1}{[(a+\rho)^2+ z^2]^{\frac{1}{2}}} \left[K + \frac{a^2-\rho^2-z^2}{(a-\rho)^2+z^2} E\right] \tag{47}$$

where μ is the permeability of free space ($4\pi \times 10^{-7}$) H/m, I is the current in amps, a is the radius of the loop and K and E are elliptic integrals of the first and second kind (Ref. 21). The values for K and E are obtained in the program using the polynomial approximations

$$K(m) = (A_0 + A_1 m_1 + \ldots + A_4 m_1^4) + (b_0 + b_1 m_1 + \ldots + b_4 m_1^4) \ln(1/m_1) \tag{48}$$

and

$$E(m) = (1 + e_1 m_1 + \ldots + e_4 m_1^4) + (d_1 m_1 + \ldots + d_4 m_1^4) \ln(1/m_1) \tag{49}$$

The values for a, b, e and d are listed in the program in Appendix A (Ref. 22). Here the parameter or modulus, m, is given by

$$m = (1-[1-k^2]^{\frac{1}{2}})\ (1+[1-k^2]^{\frac{1}{2}})^{-1} \tag{50}$$

where

$$k^2 = 4a\rho[(a+\rho)^2 + z^2]^{-1} \tag{51}$$

and

$$m_1 = 1 - m \tag{52}$$

Of course, for points on the z axis, $\rho = 0$, and $B_\rho = 0$, and $B_z = B_{tot}$ (Ref. 21).

Figure 12 shows B_z for z-axis points across the length of the coil. In Fig. 13, B_z is plotted against ρ for z = 0, 13 and 26 cm corresponding to the center, the end of the absorption cell, and just outside the coil. The fields calculated by the program are for a current of 1 A through each coil. Since the magnetic field is linear with respect to the current, simply multiplying the program result by the actual current in amps gives the magnetic field strength for that current.

The magnetic field in the z direction could not be measured inside the coil. Using a Bell* Model 640 incremental gaussmeter and a Bell HTJ-0608 probe, the field was measured just outside the coil or 26 cm from the center. The measured value of 26.5 gauss for 1 A was the same as the value obtained from the program. For a current of 9.0 A, a field of 254 gauss was measured. This was 6 percent higher than the calculated value of 238.5 gauss, but this error was less than the uncertainty in the current. The power supply used for these checks was a Sorensen** Model SRL 40-50 with a maximum output of 50 V and 50 A, and a Simpson*** Model 260 V-Ω-meter was used on the 0 to 10 A scale to measure the current. Small changes in the fine adjustment knob of the power supply caused a measurable change in the magnetic field even though the

---

* F.W. Bell, Inc., Columbus, OH 43229
Sorensen Company, Manchester, NH 03103
Simpson Electric Co., Elgin, IL 60120

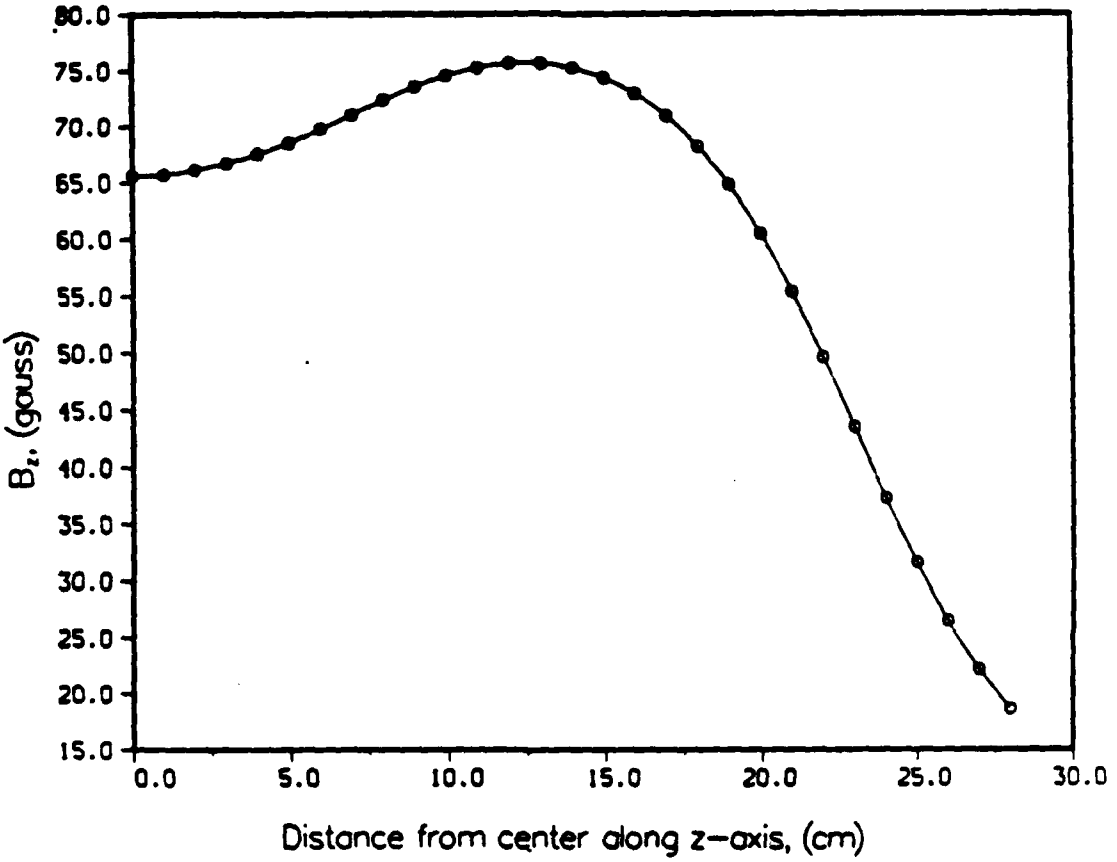

Figure 12. Magnetic field strength, B_z, along the z-axis.

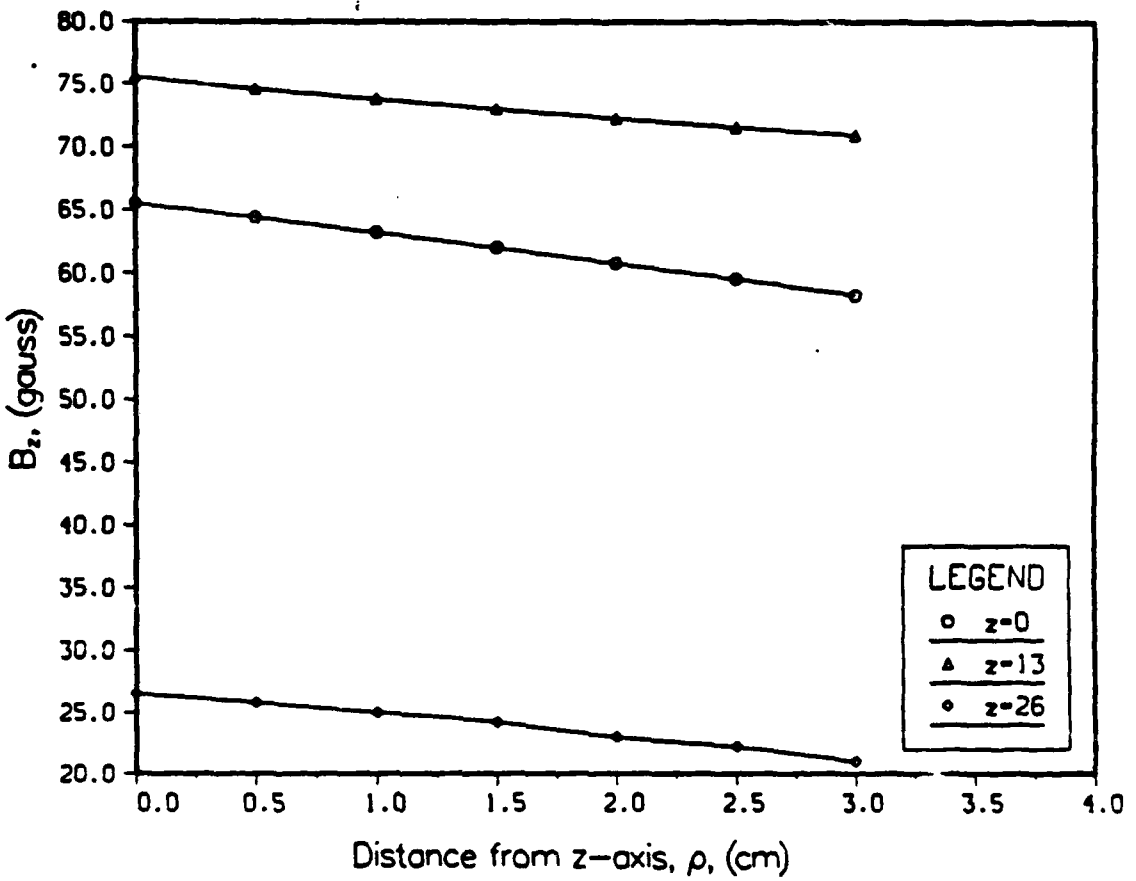

Figure 13. Magnetic field strength, B_z, for off-axis points.

reading of the current meter remained unchanged, indicating uncertainty in the current. The Gaussmeter was calibrated using a Bell Model VA-070A reference magnet with a known field of 293 gauss. A check on this calibration was performed using a current loop 6.86 cm in diameter made of 10 turns of 16 gauge copper wire. The theoretical field at the center of this loop was calculated using the well known expression

$$B_z = \frac{\mu I}{2a} = 1.83 \text{ gauss/A} \qquad (53)$$

The measured field of the test coil agreed with the calculated value to within 0.2 gauss.

Since the absorption cell was centered inside the coil, and the laser beam was aligned to within 0.5 cm of the z axis, the magnitude of B_ρ was negligible and only the z component needed to be considered. Values for B_z, on the axis, and for B_ρ 0.5 cm off the axis for a current of 1 A are given in Table 8. Once again, the field strength scales linearly with current so that the field in the absorption cell was obtained simple by multiplying the values of B_z in Table 8 by the current in amps.

The path length of the laser beam through the absorption cell was 26.5 cm. Figure 12 and Table 8 show that the magnetic field varied from 65.5 gauss/A at the center of the absorption cell to 75.6 gauss/A at each end of the absorption cell, corresponding to an average field strength across the length of the cell of 70.5 gauss/A. This was the value used to calculate the field strength for the various currents applied to the coil. The field was, therefore, approximated as uniform along the length of the absorption cell.

3.4 DATA COLLECTION

The essential features of the experimental set-up are shown in Fig. 14. The turning mirrors were 99.5 percent reflective at 1.315 μm for an incident angle of 45 deg. The beam splitter was a 40 percent reflective, 60 percent transmissive, 2.5-cm-dia pellicle. The reference beam passed through a PAR*

* Princeton Applied Research, Princeton, NJ.

TABLE 8. B_z on-axis and B_ρ 0.5 cm off-axis.

z axis Distance from center (cm)	Magnetic field (gauss/amp) B_z ρ=0	B_ρ ρ=0.5 cm
0	65.5	9.23×10^{-16}
1	65.7	0.278
2	66.1	0.530
3	66.7	0.725
4	67.5	0.830
5	68.5	0.800
6	69.7	0.587
7	71.0	0.144
8	72.3	0.563
9	73.5	1.55
10	74.5	2.79
11	75.2	4.27
12	75.6	5.94
13	75.6	7.79
14	75.2	9.78
15	74.3	11.9
20	60.5	23.5
26	26.5	25.0

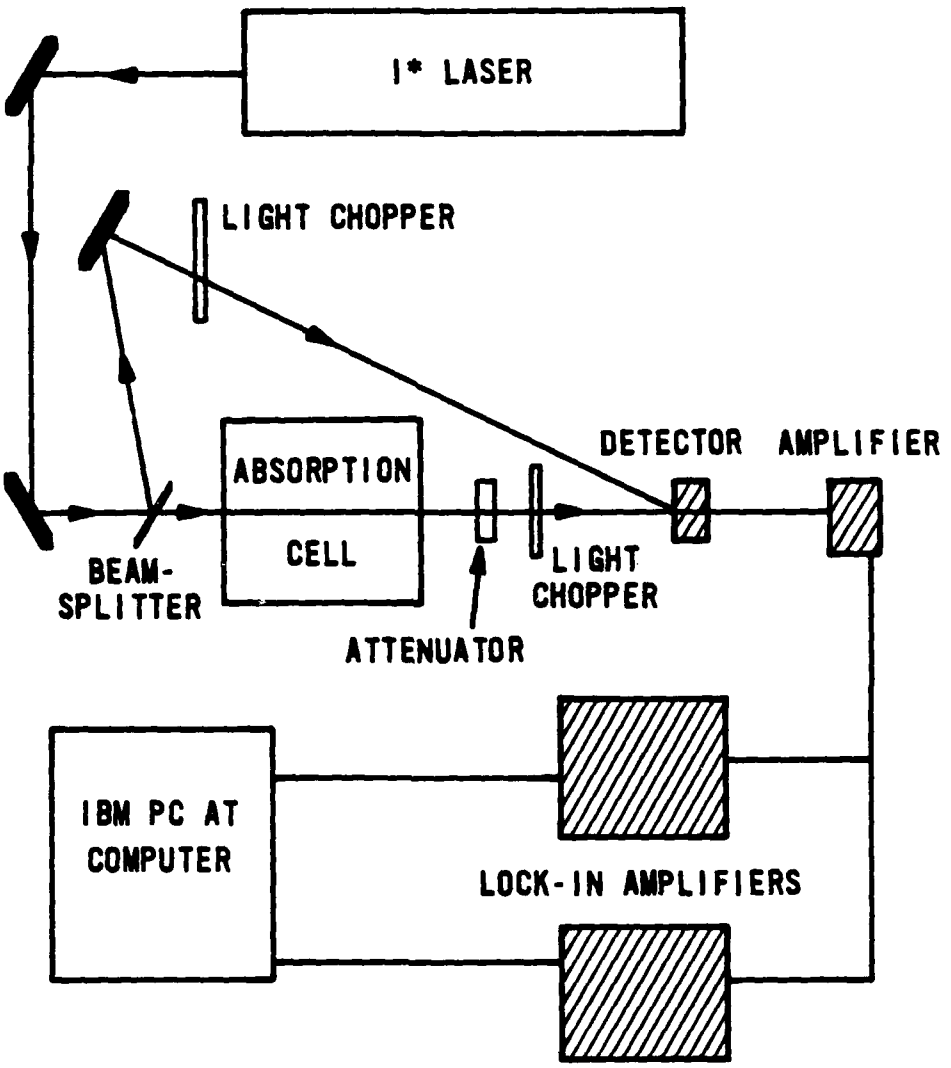

Figure 14. Experimental set-up.

Model 192 light chopper set at a frequency of 307 Hz. The absorption beam, after passing through the absorption cell, passed through an NRC* Model 925B variable attenuator and an EG&G** PARC Model 194A light chopper set at a frequency of 187 Hz. Both beams were directed onto the face of a germanium photodiode. The signal from the diode was amplified by a homemade gain-of-ten AC amplifier and sent by coaxial cable to two EG&G PARC Model 124A lock-in amplifiers with EG&G PARC Model 166 differential preamplifiers. One of the lock-in amplifiers was set at the frequency of the reference chopper and the other was set at the frequency of the absorption chopper. The variable attenuator was used to equalize the output of the two amplifiers for the case of no iodine absorption. The signals from the two amplifiers were then sent to an IBM*** PC/AT computer equipped with a Data Translation board.

The program used to acquire and reduce the signals from the amplifiers is presented in Appendix B. The program sampled the signals, divided the absorption signal by the reference signal, stored the ratio, and then took another sample. The sample rate was about 13 Hz and each run lasted 45 s for a total of 600 samples. At the end of the run, all 600 sample ratios were averaged and the average ratio for the run was displayed on the screen. Each data point reported represents an average of the ratios for at least three runs taken consecutively with constant experimental conditions.

If the ratios varied by more than 2 percent from run to run, the reason for the variance was determined and corrected. Measuring both the reference and the absorption signals on different germanium detectors resulted in variations up to 10 percent in the ratio over periods as long as 30 min. Imaging both signals onto one detector solved this problem. The iodine probe laser was a source of instability in the run ratios. While fluctuations in the laser output intensity did not in itself affect the ratio, mode shifting caused the sample ratios to vary significantly. Many things could cause mode shifting in the laser: iodine or dirt on the Brewster windows, insufficient fuel in the condenser/evaporator unit, the laser cavity pressure being too high or low, misalignment of the mirrors or iris, and the temperature of the condenser/evaporator being incorrect. A problem with the phase stability of the lock-in

* Newport Research Corporation, Fountain Valley, CA 92728
EG&G, Wellesley, MA 02181
IBM, Armonk, NY 10504

amplifiers was corrected by using Ithaco* Dynatrac Narrowband Voltmeter Model 395 amplifiers in place of the PAR Model 124As. In summary, the experimental apparatus performed quite well when the laser and detection systems were diligently monitored.

The uncertainty in the iodine source temperature (±2°C) translated into a number density uncertainty (and, hence, uncertainty in the calculated theoretical absorption values) of < 10 percent at a pressure of 1.76 torr of iodine. At higher total pressures of 6.88 and 66.7 torr, the number density uncertainty was < 5 percent. The estimated error in the absorption cell temperature, 10°C, corresponds to an additional uncertainty of 2 percent or less in the iodine number density. Due to these sources of error in the measurements, only data for conditions where the zero field absorption values are > 0.5 percent/cm will be presented.

* Ithaco, Inc., Ithaca, NY 14850

4.0 EXPERIMENTAL RESULTS AND DISCUSSION

4.1 ZERO FIELD ABSORPTION

Zero field absorption data, along with the corresponding theoretical values, are shown in Fig. 15 and tabulated in Table 9. The theoretical values were calculated using Eqs. 14, 24, 27 and 33. The pressure broadening effect on the zero field absorptions becomes apparent at pressures higher than 30 torr (Fig. 15): the plot of absorption versus number density would be linear if there were no pressure broadening effects. The number density was varied from 1.96×10^{15} (0.372 torr) to 3.55×10^{16} (66.7 torr). At the lower number densities, 2.04×10^{16} and below, the measured values correlated well with the predicted values. For the two highest number densities of 2.72×10^{16} (39.7 torr) and 3.55×10^{16} (66.7 torr), the measured absorptions were clearly less than the theoretical values. The 1.76, 6.88 and 22.9 torr zero gauss (no field) average absorption values were all within 1.5 percent of the theoretical values (Table 10). For the 39.7 and 66.7 torr cases, the average experimental values were, respectively, 3.8 and 7.0 percent below the theoretically predicted absorptions. Clearly, there appears to be a pressure broadening effect.

4.2 ABSORPTION IN A MAGNETIC FIELD

Absorption for various temperatures and pressures is plotted against magnetic field strength in Fig. 16. The corresponding data are presented in Table 10. Magnetic field strengths were determined by multiplying the applied current in amps by the average magnetic field across the length of the absorption cell for a current of one amp (70.5 gauss). The data in Figs. 16 and 17 shows that the absorption decreases with increasing magnetic field strength. All the zero field absorptions were reduced by ~ 90 percent at 635 gauss. Increasing the field from 635 to 973 gauss only reduced the absorption by an additional 4 percent so that almost all of the magnetic field effect on the absorption occurs below 635 gauss.

The absorption values presented in Fig. 16 were averaged and normalized to one, and then plotted in Fig. 17. This allows one to investigate, at least

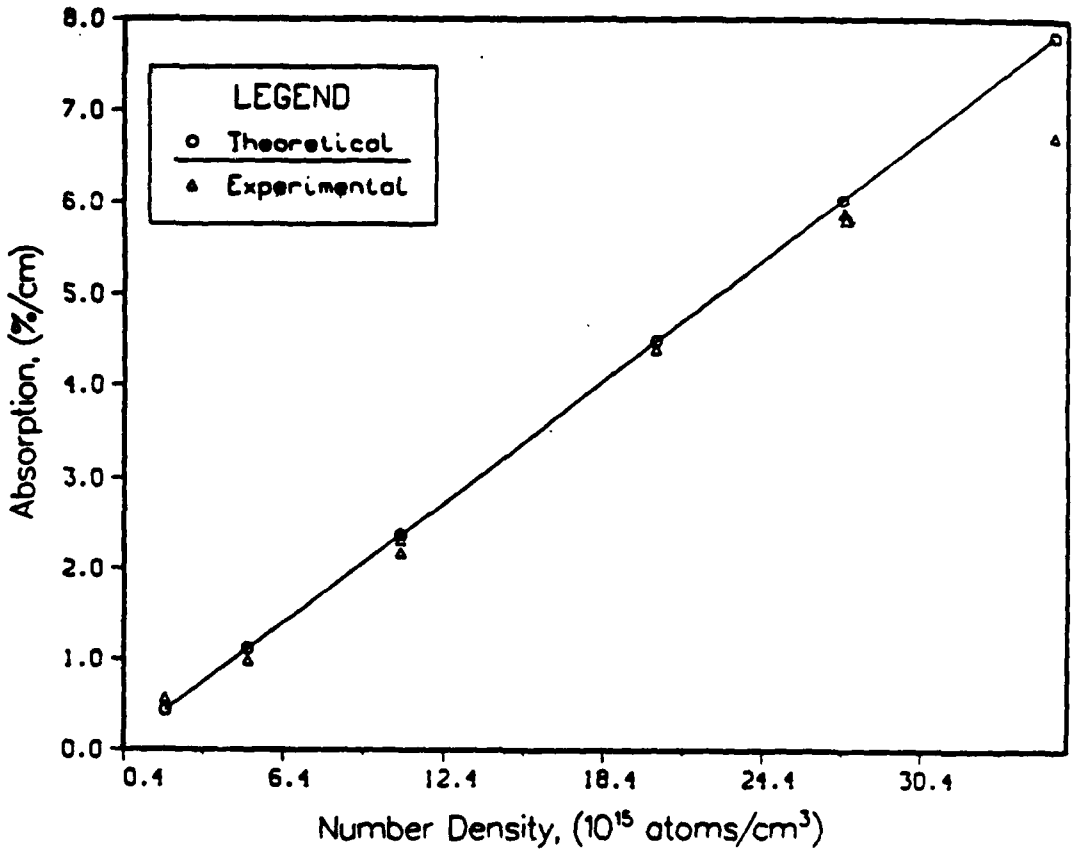

Figure 15. Absorption plotted against iodine atom number density at an absorption cell temperature of 873 K.

TABLE 9. Zero field absorption data plotted in Fig. 15.

Total Pressure (torr)	Absorption Cell Temperature (K)	Iodine Atom Number Density ($atoms/cm^3$)	Absorption (%/cm)
0.372	873	1.96×10^{15}	0.432 [a]
"	"	"	0.570
1.76	"	5.08×10^{15}	1.119 [a]
"	"	"	0.99
6.88	"	1.08×10^{16}	2.378 [a]
"	"	"	2.18
"	"	"	2.32
"	"	"	2.40
22.9	"	2.04×10^{16}	4.49 [a]
"	"	"	4.40
39.7	"	2.72×10^{16}	5.99 [a]
"	"	"	5.84
"	"	"	5.73
"	"	"	5.71
66.7	"	3.55×10^{16}	7.82 [a]
"	"	"	6.74

[a]Theoretical values from Table 5.

TABLE 10. Absorption data (%/cm) versus magnetic field plotted in Fig. 16.

	Cell Temperature (k) / Total Pressure (torr)				
Magnetic Field	823	823	898	873	823
(gauss)	1.76	6.88	22.9	39.7	66.7
0	0.69[a]	1.42[a]	4.99[a]	5.99[a]	4.56[a]
0	0.68	1.44	5.06	5.84	4.23
0	0.68	1.42	5.06	5.73	4.31
0		1.38	4.93	5.71	4.20
0		1.40	5.00		4.25
70.5		1.30	4.68	5.35	3.94
70.5		1.31	4.56	5.23	3.86
70.5		1.30	4.56	5.33	3.89
70.5			4.44		3.90
70.5			4.44		3.95
70.5			4.33		
141	0.46	0.86	3.19	3.73	3.01
141	0.43	0.83	3.19	3.72	3.00
141	0.41	0.86	3.19	3.76	3.00
141		0.82	3.19	3.76	
211.5		0.52	2.25	2.67	2.12
211.5		0.48	2.25	2.72	2.16
211.5		0.49	2.22	2.69	2.17
211.5		0.52	2.22	2.70	2.15
282	0.18	0.34	1.66	1.98	1.67
282	0.19	0.34	1.66	2.00	1.67
282	0.19	0.34	1.66	2.02	1.66
352.5		0.23	1.30	1.49	1.35
352.5		0.23	1.30	1.50	1.34
352.5		0.27	1.30	1.49	1.34
423	0.08	0.20	1.06	1.23	1.07
423	0.12	0.16	1.06	1.23	1.07
423	0.08	0.16	1.06	1.24	1.09
493.5		0.16	0.92	.99	0.88
493.5		0.16	0.87	0.97	0.90
493.5		0.12	0.92	0.99	0.91
564	0.07	0.12		0.83	0.74
564	0.07	0.12		0.86	0.74
564	0.08	0.12		0.83	0.77
634.5	0.07	0.09	0.70	0.71	0.67
634.5	0.04	0.05	0.70	0.69	0.69
634.5	0.05	0.05		0.67	0.71
775.5			0.58		
775.5			0.58		
973			0.49		
973			0.49		

[a] Theoretical values.

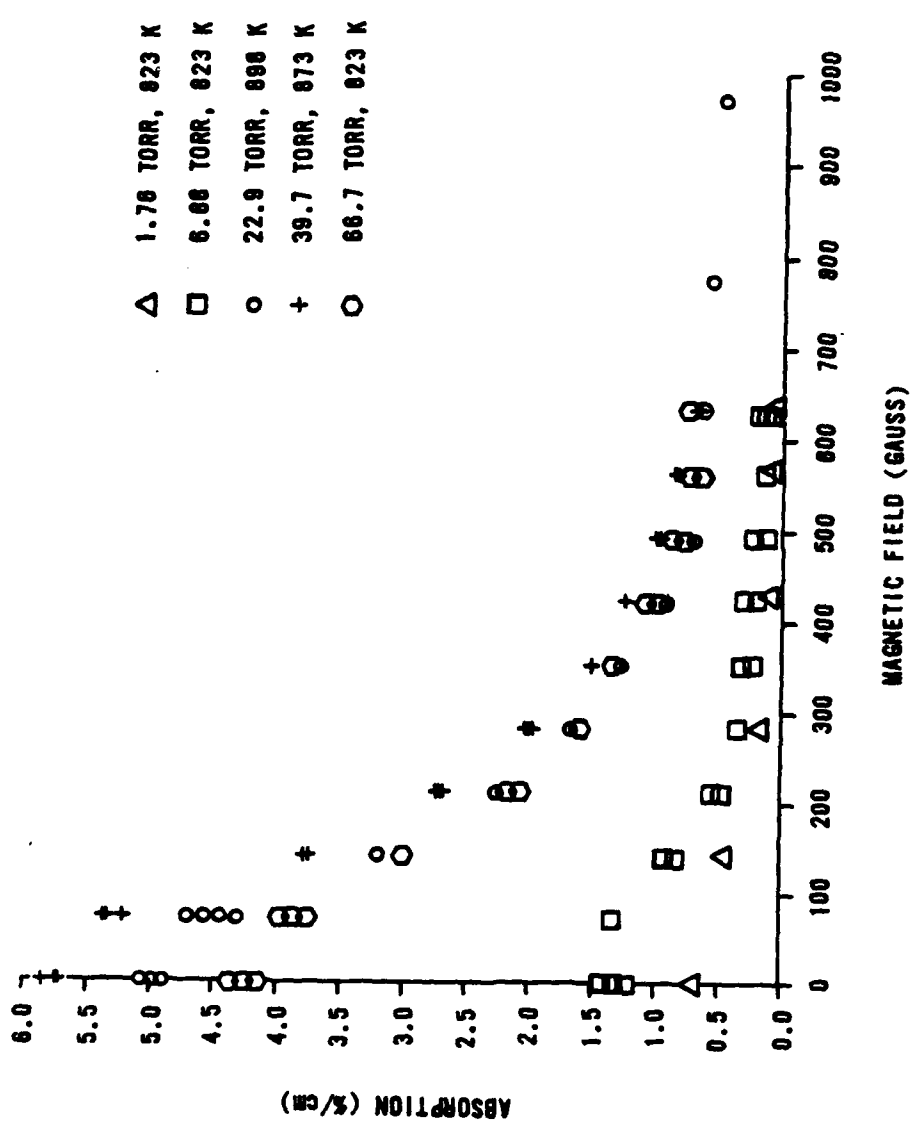

Figure 16. Absorption plotted against magnetic field strength.

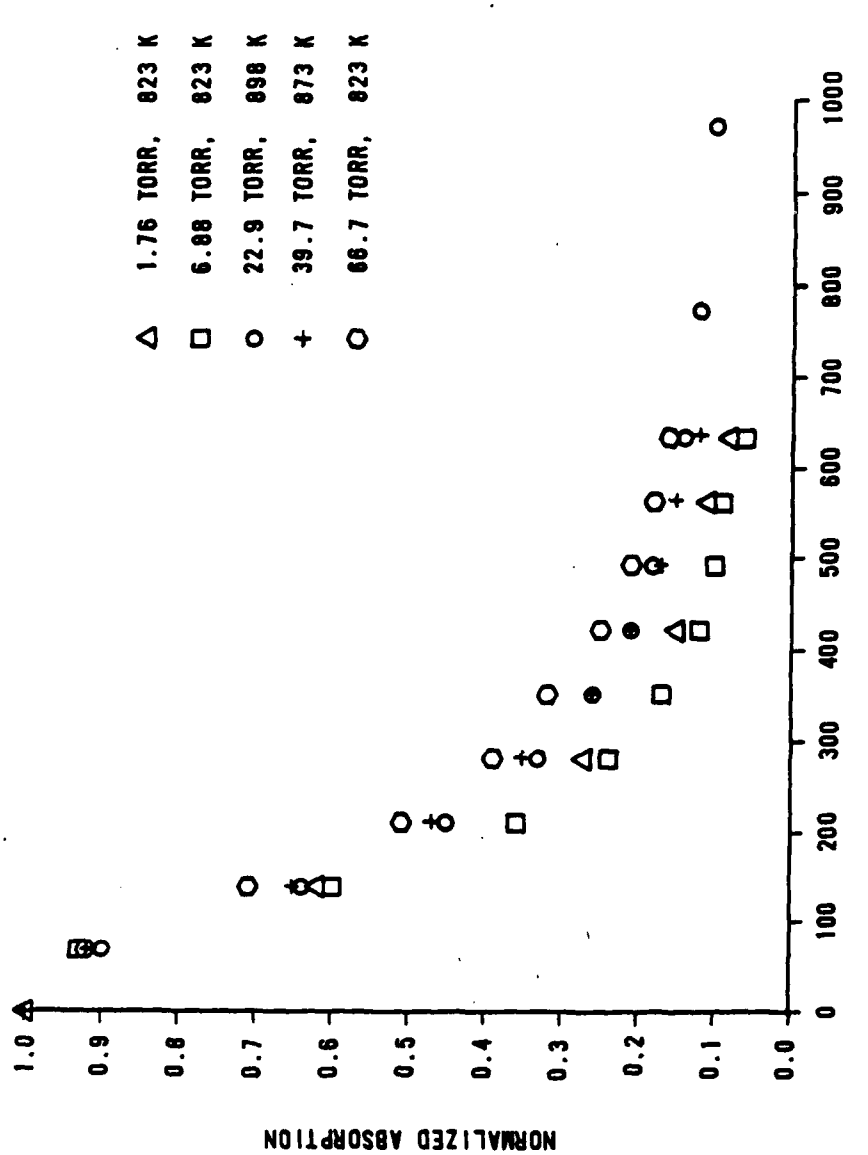

Figure 17. Normalized absorption versus magnetic field strength.

qualitatively, the effects of pressure on the ability of a magnetic field to reduce absorption. As can be seen in the figure, the low pressure absorptions are reduced by about 90 percent at 635 gauss while the high pressure absorptions are reduced by only about 85 percent at 635 gauss. Because of uncertainty in the absorptions at these field strengths, this observation should be considered qualitative, not quantitative.

The fact that the magnetic field had less effect on the higher pressure cells than on the lower pressure ones can be explained. From Table 7, the Doppler broadened line width at 823 K is 416 MHz, which is the actual line width because pressure broadening is negligible at 1.76 torr, and, recall that the pressure broadening coefficient for atomic iodine is 1.3 MHz/torr and is 3.1 MHz/torr for molecular iodine (Ref. 14). From Ref. 3 and calculations performed at AFWL, only the weak 2,1; -1,0; 1,0; and -2, -1 hyperfine transitions are close enough to the laser transition to contribute significantly to the absorption in a magnetic field of 635 gauss. On the other hand, the Voigt line width at 66.7 torr and 823 K is 499 MHz, so that the 0, 1 and 0, -1 hyperfine transitions may be broadened enough to also contribute to the absorption at the laser transition energy, and so it makes qualitative sense that the broader overlapping lines would result in the magnetic field having less of an effect on the laser line absorption.

5.0 CONCLUSIONS AND RECOMMENDATIONS

Absorption of 1.315 μm radiation by atomic iodine was reduced in the presence of a magnetic field because of Zeeman splitting of the iodine hyperfine levels. The absorption decreased as the magnetic field increased. The amount of absorption reduction for a given magnetic field showed no apparent dependence on the temperature of the absorption cell over the range investigated (823 to 873 K). For those cases where the total pressure was 22.9 torr or less, the absorption was reduced by roughly equal factors for equal magnetic fields. Because of pressure broadening effects on the magnetic hyperfine transition line-widths at a total pressure of 66.7 torr, the absorption was reduced by proportionally smaller amounts compared with low pressure cases for equivalent magnetic field strengths. A qualitative theoretical model was developed for the purpose of analyzing the experimental results.

The zero field absorption data were in agreement with the theoretically predicted values. Measurements of high absorption values were more precise than measurements of low absorption values which were prone to unacceptably large fluctuations from run-to-run. Uncertainties in the absorption data were the result of shortcomings in the experimental apparatus.

A longer cell would allow one to measure absorption for lower number densities with the same experimental apparatus. Lengthening the cell would give higher total absorptions than would a shorter cell under equivalent conditions, resulting in better signal/noise ratios.

Eliminating all o-ring seals would be advantageous in the sense that it would reduce the probability of leaks in the system. A closed system would have an added advantage in that the problem of cold spots in the supply line could be eliminated simply by heating the supply line well above the brass block temperature, without concern for melting the o-ring seals.

REFERENCES

1. Kasper, J.V.V.; and Pimentel, G.C.; "Atomic Iodine Photo-dissociation Laser," Appl Phys. Lett. 5, pp. 231-233 (1964).

2. Gray, D.R.; Baker, H.J.; and King, T.A.; "Atomic Absorption of Thermally Dissociated Iodine for Laser Applications," J. Phys. D: Applied Phys., 10, pp. 169-177 (1977).

3. Belousova, I.M.; Bobrov, B.D.; Kiselev, V.M.; Kurzenkov, V.N.; and Krepostnov, P.I.; "I^{127}Atom in a Magnetic Field," Opt. Spectrosc., 37, pp. 20-24 (1974).

4. Kubaschewski, O.; and Evans, E.; Metallurgical Thermochemistry, John Wiley and Sons, New York, NY (1956).

5. Herzberg, G., Spectra of Diatomic Molecules, 2nd Ed., Van Nostrand, New York, NY (1950).

6. Münster, Statistical Thermodynamics, Vol. 1, Academic Press, New York, NY, pp. 440-483 (1969).

7. Tellinghuisen, J.; McKeever, M.R.; and Sur, A.; "Reanalysis of the D→X Fluorescence Spectrum of I_2," J. Mol. Spec. 82, pp. 225-245 (1980).

8. DeVries, T., and Rodebush, W.H.; "The Thermal Dissociation of Iodine and Bromine," J. Am. Chem. Soc., 49, pp. 656-666 (1927).

9. Perlman, M.L., and Rollefson, G.K.; J. Chem. Phys., 9, pp 362-369 (1941).

10. Bransden, B.H., and Joachain, C.J.; Physics of Atoms and Molecules, Longman, White Plains, NY (1983).

11. Engleman, R.; Keller, R.A.; and Palmer, B.A.; "Hyperfine Structure and Isotope Shift of the 1.3 μm Transition of ^{129}I," Appl. Opt. 19, pp. 2767-2770 (1980).

12. Lederer, C.M., and Shirley, V.S.; Table of Isotopes, Seventh Edition, Appendix VII, John Wiley and Sons, New York, NY (1978).

13. Zuev, V.S.; Katulin, V.A.; Nosach, V. Yu.; and Nosach, O. Yu, "Investigation of the Luminescence Spectrum of Atomic Iodine ($^2P_{1/2} \rightarrow {}^2P_{3/2}$ laser transition:," Sov. Phys. JETP 35, pp. 870-873 (1972).

14. Engleman, R., Jr.; Palmer, B.A.; and Davis, S.J.; "Transition Probability and Collision Broadening of the 1.3 μm Transition of Atomic Iodine," J. Opt. Soc. Am., 73, No. 11, pp. 1585-1589 (1983).

15. Davies, J.T., and Vaughan, J.M.; "A New Tabulation of the Voigt Profile," Astrophysical Journal, 137, pp. 1302-1305 (1963).

REFERENCES (Concluded)

16. Schlie, L.A., and Rathge, R.D.; "Long Operating Time CW Atomic Iodine Probe Laser at 1.315 microns," IEEE J. Quant. Elect., QE-20, pp. 1187-1196 (1984).

17. Schlie, L.A., and Rathge, R.D.; "Closed-cycle Gaseous Alkyl-iodide (C_3F_7I) Supply System," Rev. Sci. Instrum., 55, No. 4, pp.482-485 (1984).

18. Rathge, R.D., Personal Conversations with Authors, Air Force Weapons Laboratory/ARBI, Kirtland AFB, NM 87117-6008 (May 1986).

19. Richert, S., and Herrera, S.; Personal Conversations with Authors, Air Force Weapons Laboratory, Kirtland AFB, NM 87117-6008 (May 1986).

20. Derwent, R.G.; Kearns, D.R.; and Thrush, B.A.; Chem. Phys. Lett., 6, pp. 115-116 (1970).

21. Smythe, W.R., Static and Dynamic Electricity, third ed., McGraw Hill, New York, NY, 291 (1968).

22. Abramowitz, M., and Stegun, I.A.; Handbook of Mathematical Functions, sixth ed., U.S. Dept. of Commerce, National Bureau of Standards, Wash, DC, pp. 591-592 (1967).

APPENDIX A
COMPUTER PROGRAM FOR CALCULATING
THE MAGNETIC FIELD OF A SOLENOID

Written by: J.P. O'Loughlin

```
SOURCE
 10  REM PGM NAME IS BCALC1.BAS, CALS B FIELD OF A SOLENOID
 20  REM CONFIG OF SOL HAS THREE SECTIONS, TWO ENDS OF LENGTH EL AND
 30  REM DIA ED AND A MIDDLE SECTION OF LENGTH ML AND DIA MD
 40  REM THE TURNS IN EACH END ARE ET AND IN MIDDLE MT
 50  REM A TEST CURRENT OF ONE AMP IS ASSUMED
 60  REM THE B(RHO) , B(Z) AND TOTAL FIELDS ARE CLAC USING
 70  REM ELIPTIC INTERGALS E AND K
 80  REM THE ORIGIN IS THE CENTER OF THE MIDDLE SECTION
 90  PIE=3.14159265358979323846264 3
100  INPUT" ENTER LENGTH OF END SECTION " EL
102  LPRINT"LENGTH OF END SECTION ="EL"METERS"
110  INPUT" ENTER LENGTH OF MIDDLE SECTION " ML
112  LPRINT"LENGTH OF THE MIDDLE SECTION="ML "METERS"
120  INPUT" ENTER THE OUTER DIA OF END SECTION" ODE
121  INPUT" ENTER THE INNER DIA OF END SECTION" IDE
122  LPRINT"OUTER DIA OF END SECTIONS="ODE"METERS"
124  LPRINT"INNER DIA OF END SECTIONS="IDE"METERS"
130  INPUT" ENTER THE OUTER DIA OF THE MIDDLE SECTION" ODM
131  INPUT" ENTER THE INNER DIA OF THE NIDDLE SECTION" IDM
132  LPRINT"OUTER DIA OF MIDDLE SECTION="ODM"METERS"
134  LPRINT"INNER DIA OF MIDDLE SECTION="IDM"METERS"
140  INPUT" ENTER NUMBER OF TURNS PER LAYER OF END SECTION " ENL
141  LPRINT" NUMBER OF TURNS PER LAYER OF END SECTION = "ENL"TURNS/LAYER"
150  INPUT" ENTER NUMBER OF TURNS PER LAYER OF MIDDLE SECTION " MNL
151  LPRINT"NUMBER OF TURNS PER LAYER OF MIDDLE SECTION="MNL"TURNS/LAYER"
160  INPUT" ENTER NUMBER OF TOTAL TURNS OF END SECTION " ET
161  LPRINT"TOTAL NUMBER OF TURNS IN END SECTION="ET"TURNS"
170  INPUT" ENTER NUMBER OF TOTAL TURNS OF MIDDLE SECTION"MT
171  LPRINT"TOTAL NUMBER OF TURNS IN MIDDLE SECTION="MT"TURNS"
180  ELAYERS=ET/ENL
181  LPRINT"NUMBER OF LAYERS IN END SECTION="ELAYERS"LAYERS"
190  MLAYERS=MT/MNL
191  LPRINT"NUMBER OF LAYERS IN MIDDLE SECTION="MLAYERS"LAYERS"
200  INPUT "ENTER NUMBER OF Z AXIS CALC POINTS" NZ
210  INPUT "ENTER THE SPACING OF THE Z AXIS CALC POINTS " SZ
230  INPUT "ENTER THE SPACING OF THE RHO POINTS" SRHO
231  INPUT" ENTER THE NUM OF RHO POINTS" NRO
240  FOR NNRO=0 TO NRO
250     RHOCAL = NNRO*SRHO
260     FOR NNZ=0 TO NZ
270       ZCAL=NNZ*SZ
271       BZ=0:BTOT=0:BRHO=0
280       REM CAL LEFT AND RIGHT END COMPS
290       FOR NLAYER=1 TO ELAYERS
300         A=IDE/2+(NTL-.5)*(ODE-IDE)*.5/ELAYERS
310         FOR NTL=1 TO ENL
```

```
320          ZLE=+ML/2+(NTL-.5)*EL/ENL  +ZCAL
330          ZRE=-ML/2+ZCAL-(NTL-.5)*EL/ENL
340          K2L=4*A*RHOCAL/((A+RHOCAL)^2+ZLE^2)
350          K2R=4*A*RHOCAL/((A+RHOCAL)^2+ZRE^2)
360          M=(1-(1-K2L)^.5)/(1+(1-K2L)^.5)
370          GOSUB 1000
372          RHO=RHOCAL
373          Z=ZLE
380          GOSUB 2000
390          M=(1-(1-K2R)^.5)/(1+(1-K2R)^.5)
400          GOSUB 1000
402          Z=ZRE
410          GOSUB 2000
420        NEXT NTL
422      NEXT NLAYER
430      FOR NLAYER=1 TO MLAYERS
440        A=IDM/2+(NLAYER-.5)*(ODM-IDM)*.5/MLAYERS
450        FOR NTL=1 TO MNL
460          ZM=ZCAL+ML/2-(NTL-.5)*ML/MNL
470          K2M=4*A*RHOCAL/((A+RHOCAL)^2+ZM^2)
480          M=(1-(1-K2M)^.5)/(1+(1-K2M)^.5)
490          GOSUB 1000
500          Z=ZM
510          GOSUB 2000
520        NEXT NTL
530      NEXT NLAYER
540      BTOT=(BZ*BZ+BRHO*BRHO)^.5
541      BTOT=BTOT*2E-7:BZ=BZ*2E-7:BRHO=BRHO*2E-7
550      LPRINT "Z="ZCAL,"RHO="RHOCAL, "BZ="BZ, "BRHO="BRHO,"BTOT="BTOT
560    NEXT NNZ
570  NEXT NNRO
580  END
1000 REM CALCULATION SUBROUTINE FOR ELLIPTIC FIRST AND SECOND INT OF M1
1005 M1=1-M
1006 IF QZ>0 THEN GOTO 1110
1010 A0=1.38629436112
1020 A1=.09666344259
1030 A2=.03590092383
1040 A3=.03742563713
1050 A4=.01451196212
1060 B0=.50000000000
1070 B1=.12498593597
1080 B2=.06880248576
1090 B3=.03328355346
1100 B4=.00441787012
1110 KM=A0+A1*M1+A2*M1^2+A3*M1^3+A4*M1^4
1120 KM=KM+(B0+B1*M1+B2*M1^2+B3*M1^3+B4*M1^4)*LOG(1/M1)
1121 IF QZ>0 THEN GOTO 1120
1130 REM CALCULATE SECOND ELLIPTIC FN OF M,M1
1140 E1=.44325141463
1150 E2=.06260601220
1160 E3=.04757383546
1170 E4=.01736506451
```

```
1180  D1=.24998368310
1190  D2=.09200180037
1200  D3=.04069697526
1210  D4=.00526449639
1211  QZ=1
1220  EM=1+E1*M1+E2*M1^2+E3*M1^3+E4*M1^4
1230  EM=EM+(D1*M1+D2*M1^2+D3*M1^3+D4*M1^4)*LOG(1/M1)
1240  RETURN
2000  REM SUB PGM FOR CAL BRHO AND BZ
2020  BZ=BZ+(KM+EM*(A*A-RHO*RHO-Z*Z)/((A-RHO)^2+Z*Z))/((A+RHO)^2+Z*Z)^.5
2022  IF RHO=0 THEN GOTO 2040
2030  BRHO=BRHO+Z/RHO*((A+RHO)^2+Z*Z)^.5)*(-KM+(A*A+RHO*RHO+Z*Z)*EM/(
      ((A-RHO)^2+Z*Z))
2040  RETURN
ENDFILE
```

APPENDIX B
COMPUTER PROGRAM FOR DATA COLLECTION

Written by: Leonard Hanko

```
  5  RATIO=0
 10  DIM DET1(2000),DET1%(2000),DET2%(2000),M$(100)
 20  N=25
 30  Q$=" "
 40  KEY OFF
 50  SCREEN 0
 60  COLOR 14,9,0:CLS
 65  GOSUB 1790
 70  PRINT DATE$
 80  PRINT TIME$
 90  REM*********************************
100  REM  GET DATE AND FIRST RUN # FOR DAY
110  REM*********************************
120  PRINT TAB(N);:INPUT "RUN # TO START WITH  ";Q
130  Q1$=STR$(Q)
140  Q=Q-1
150  PRINT "THis will be first file written  ";F1$+Q1$
160  FOR I=1 TO 7 :PRINT :NEXT I
170  SCREEN 0:COLOR 14,1,0
180  CLS
190  PRINT TAB(N);"DATA ACQUIRING OPTIONS"
200  PRINT TAB(N-5);" 1)  Set up channels"
210  PRINT TAB(N-5);" 2)  Scan information"
220  PRINT TAB(N-5);" 3)  Aquire data"
230  PRINT TAB(N-5);" 4) Save data"
240  PRINT TAB(N-5);" 5) EXIT PROGRAM"
250  PRINT TAB(N);:INPUT "ENTER CHOICE";ANS%
260  IF ANS%(0 THEN GOTO 170 ELSE IF ANS%>5 THEN GOTO 170
270  ON ANS% GOSUB 300,350,410,490,650
280  IF FLAG=1 THEN FLAG=0:RETURN
290  GOTO 170
300  REM*****************SET UP CHANNELS***************
310  CLS
320  PRINT TAB(N);;INPUT  "Gain for DETECTOR 1=(0,1,2,3)";GAIN1%
325  PRINT TAB(N);;INPUT  "Gain for detector 2";GAIN2%
330  REM
340  RETURN
350  REM*************DATA TO FILE*****************
351  PRINT TAB(N);;INPUT  "What is Iodine cell temp (deg C)";M1$
352  PRINT TAB(N);;INPUT  "What is the absorption cell temp (degC)";M2$
353  PRINT TAB(N);;INPUT  "What is magnetic field strength (gauss)";M3$
355  M$=M1$+Q$+M2$+Q$+M3$
356  IF LEN(M$)>40 THEN GOTO 350
370  PRINT M$
380  IF ANS$="Y" THEN GOTO 400 ELSE IF ANS$="N" GOTO 360
400  RETURN
410  REM***************SUB TO ACQUIRE DATA****************
420  IF ANS$="Y" THEN GOTO 440
```

```
430  IF ANS$="N" THEN GOTO 950
440  PRINT TAB(N):INPUT "PRESS ANY KEY TO START";A$
450  CLS
460  SCR%=1
470  GOSUB 660
480  RETURN
490  REM**********************OPTIONAL DATA SAVE TO DISK*********
500  CLS
510  PRINT TAB(N);:INPUT "DO YOU WISH TO SAVE THE DATA";ANS$
520  IF ANS$="N" THEN GOTO 640
530  IF ANS$="Y" THEN GOSUB 1720 ELSE PRINT "WRONG INPUT(Y OR N)":GOTO
     510
540   F$="DATA/"+F1$+Q1$+".DAT"
550  OPEN F$ FOR OUTPUT AS #2
560   NPT$=STR$(NPNTS%)
565  RATIO$=STR$(RATIO)
570  M$=NPT$+Q$+RATIO$+Q$+M$
580  PRINT #2,M$
590  PRINT "WRITING TO FILE ";F$
600  FOR I%=1 TO NPNTS%
610  PRINT #2,DET1%(I%);DET2%(I%)
620  NEXT 1%
630  CLOSE #2
640  RETURN
650  END
660  REM Start experiment
665  GOSUB 1410
670  REM************************************************************
680  NPNTS%=600
690  SCR%=1
695  GOSUB 1460
700  PRINT TAB(20);"aquiring points",NPNTS%
710  FOR I%=1 TO NPNTS%
715      IF I%)(SCR%*600) THEN CLS:SCR%=SCR%+1:GOSUB 1460
720    SUM=0
730       D%=0
740       CHANNEL%=1
750       GAIN%=GAIN1%
760       GOSUB 1040
770       DET1%(I%)=D%
775  CHANNEL%=2
778  GAIN%=GAIN2%
780  GOSUB 1040
785      DET2%(I%)=D%
830      DET1=DET1%(I%)  :DET2=DET2%(I%)
835      TEMP=(DET1/DET2)
836  TEMP=TEMP/2
840      YPOINT%=190!-(TEMP)*180!
850      XPOINT%=I%-((SCR%-1)*600)+19
860      LINE -(XPOINT%,YPOINT%)
870      PSET(XPOINT%,YPOINT%)
880  LOCATE 1,35
890  PRINT "      ";
```

```
 895  RATIO=RATIO+TEMP
 897  LOCATE 25,10:PRINT TIME$,
 900      NEXT I%
 905  RATIO=(RATIO/600) *2
 910  LOCATE 1,22:PRINT RATIO;
 920  LOCATE 1.1
 930  BEEP
 940  INPUT ; ABC$
 950  ABC$=INKEY$:IF ABC$=" " THEN GOTO 950
 960  CLS
 970  RETURN
 980  END
 990  REM*******************************************************
1000  REM*******************************************************
1010  REM This routine reads the a/d converter and returns the
1020  REM result in the variable data%
1030  REM*******************************************************
1040  COMMAND%=12
1050  GOSUB 1180
1060  COMMAND%=GAIN%
1070  GOSUB 1250
1080  COMMAND%=CHANNEL%
1090  GOSUB 1250
1100  GOSUB 1340
1110  D%=X1%
1120  GOSUB 1340
1130  D%=D%+X1%*256
1140  RETURN
1150  REM*********************************************************
1160  REM This routine performs a simple write to the command register
1170  REM*********************************************************
1180  WHILE((INP(&H2ED) and 6) <>4)
1190  WEND
1200  OUT &H2ED, COMMAND%
1210  RETURN
1220  REM*********************************************************
1230  REM This routine performs a simple write to the data register
1240  REM*********************************************************
1250  WHILE  ((INP(&H2ED) AND 2)=2
1260  WEND
1270  OUT &H2EC,COMMAND%
1280  RETURN
1290  REM*******************************************************
1300  REM THis routine reads from the data register and returns 1 byte
1310  REM in x1%
1320  REM The routine must be called twice to complete the read.
1330  REM*******************************************************
1340  WHILE((INP(&H2ED) AND 1)<>1)
1350  WEND
1360  x1%=INP(&H2EC)
1370  RETURN
1380  REM*********************************************************
1390  REM This routine clears the a/d registers prior to first use
```

```
1400  REM*******************************************************
1410  IF (INF(&H2ED) AND 1)=1 THEN DUM%=INP(&H2EC)
1420  RETURN
1430  REM*******************************************************
1440  REM  Draw Axis
1450  REM*******************************************************
1460  SCREEN 2
1470  LOCATE 1,3
1480  PRINT F$;
1490  LINE (20,10)-(20,190)
1500  LINE (20,190)-(620,190)
1510  LINE (620,190)-(620,10)
1520  LINE (620,10)-(20,10)
1530  REM*******************************************************
1540  REM Draw tic marks on x axis
1550  REM*******************************************************
1560  FOR G%=20 TO 600 STEP 60
1570     LINE (G%,192)-(G%,185)
1580     WLLABEL=(G%-20)*INC+WLSTART+((SCR%-1)*600*INC)
1590     WLLABEL$=STR$(WLLABEL)
1600     LABPOS%=G%/8-2
1610     LOCATE 25,LABPOS%
1620     PRINT USING "/   /"; WLLABEL$;
1630     NEXT
1640  G%=G%-60
1650  LINE -(G%,190)
1660  LINE -(20,190)
1670  LOCATE 1,1
1680  RETURN
1700  Print "Input any key to return to menu";
1710  IF LEN(MT$))90 THEN GOTO 350
1720  REM**********REMOVES SPACE FROM FILE NAME*************
1730  T$=CHR$(32)
1740  Q=Q+1:Q1$=STR$(Q)
1750  IF INSTR(Q1$,T$) > 0 THEN P1=INSTR(Q1$,T$)
1760  Q1$=MID$(Q1$,(P1+1))
1770  IF LEN(Q1$)=1 THEN Q1$="0"+Q1$
1780  RETURN
1790  REM********VERIFY DATE IS CORRECT**********************
1800  FOR I%= 1 to 3
1810  F$(I%)=MID$(DATE$,I%^2,2)
1820  NEXT I%
1830  F$=F$(1)+F$(2)+F$(3)
1840  F1$=F$
1850  RETURN
```